SUPERFLUIDITY OF LIGHT

Report for 3rd Year Internship

Option	Département de Physique
Champ	Physique de la Matière Condensée
Enseignant référent	Luca PERFETTI
Tuteur de stage	Quentin GLORIEUX
Dates	14 mars 2016-15 août 2016
Organisme	Laboratoire Kastler Brossel

Dhruv SHARMA-Promotion X2013
P.A. Des Particules aux Étoiles

l'X
ÉCOLE POLYTECHNIQUE
UNIVERSITÉ PARIS-SACLAY

Abstract

In English

Quantum simulation experiments have garnered tremendous excitement over the past few years. They provide us a tremendous tool to understand many-body quantum phenomena without resorting to exotic computer simulations or complicated theoretical calculations. Superfluidity is one phenomenon which has lent itself really well to such an approach with the development of polaritonic systems in microcavity configurations. However, these experiments are usually experimentally complicated. We devise a new method to study the quantum phenomena of superfluidity using a well understood optical system: the propagation of light in a non-linear medium exhibiting a third-order non-linearity. Using a pump-probe technique, we observe the Boguliobov dispersion relation for elementary excitations in a superfluid, but with light. Conducted at room temperature, this presents the first demonstration of an experiment demonstrating the propagation of light as a quantum fluid.

En Français

Les expériences de simulation quantique ont suscité un énorme enthousiasme au cours des dernières années. Ils nous fournissent un formidable outil pour comprendre les phénomènes quantiques à plusieurs corps sans avoir recours à des simulations informatiques exotiques ou des calculs théoriques complexes. Superfluidité est un phénomène qui se prête très bien à une telle approche avec le développement de systèmes polaritonic dans des configurations de microcavité. Toutefois, ces expériences sont généralement compliquées à mettre en oeuvre. Nous élaborons une nouvelle méthode pour étudier les phénomènes quantiques de superfluidité en utilisant un système optique bien compris: la propagation de la lumière dans un milieu non-linéaire. En utilisant une technique pompe-sonde, on observe la relation de dispersion de Boguliobov pour des excitations élémentaires dans un superfluide, mais avec la lumière. Conduite à la température ambiante, cela présente la première démonstration d'une expérience démontrant la propagation de la lumière comme un fluide quantique.

Acknowledgements

The last five months that I spent at LKB were a supremely enriching experience for me. I would thus like to first of all thank my tutor Dr. Quentin Glorieux, who proposed the topic of my internship. I would like to sincerely thank him for accepting me for this internship.

Having no prior experience in experimental physics, my baptism by fire was tempered by the experience of Dr. Glorieux, who helped me understand the basic aspects of the experiment. I would also like to thank Stefano Pierini, with whom I worked for the first three months. Stefano showed immense patience with me in explaining the functioning of the various elements of the experiment. I would like to thank him for never once losing his cool over the course of numerous debates on a whole host of topics, from the correct way of taking data to the optimal orientation of the rubidium cell.

I also had the chance to interact with Mathieu Durand who helped me out whenever there was a problem with the laser. I would like to make a special mention of Tanguy Aladjidi, who impressed me with the vivacity of spirit which will bode him well for the next stage of his studies at Ecole Polytechnique.

The internship wouldn't have been the same without regular cups of coffee. For this, a special mention to Maxime Joos, a PhD student in the nano-fibers group, who managed the stock of coffee for all interns and PhD students at LKB, UPMC. I would also like to thank Vivien for accompanying me over long lunches taken together, when he calmly listened to whatever I had to say. He was always present whenever I encountered a problem with the laser (which was often).

A special thanks to Iacopo Carosutto, who had the idea for the experiment and who responded to all my queries pertaining to theoretical questions.

Finally, I would like to thank Alberto Bramati, group leader for being available to point out some subtle point or the other during team meetings.

CONTENTS

LIST OF FIGURES

Part I

Introduction

The phenomenon of superfluidity has a long and rich history. First discovered in liquid helium, the superfluid character of ^{4}He was first demonstrated independently by Allen and Misener [1] and Kapitza [2] in 1938. Fritz London, then working at College de France was the first to figure out that the so called λ point T_λ of 2.17K for ^{4}He is rather close to the critical temperature for a BEC transition T_c for an ideal Bose gas, at the same density [3]. This was the first suggestion for the link between the phenomenon of Bose-Einstein Condensation(BEC) and superfluidity.

The link between superfluidity and BEC however, is not a simple one to unravel. It has been shown that in superfluid Helium, only about 10% of atoms are in the condensed state. What is certain however is, that for the presence of superfluid character, it is important that the system be bosonic. Even ^{3}He, which is a fermion, behaves as a superfluid, by forming a pair with another ^{3}He atom. The presence of a bosonic state is not the only criteria for superfluidity. Another ingredient is interactions. Interactions make the physics more complicated but very interesting too.

A rather obvious question to ask is the following: what of the bosons that are rather ubiquitous in nature and also in labs all over the world, photons? That would indeed be a valid question, because photons are in effect bosons, par excellence: they are fundamental bosons, in contrast to the composite bosons which are *de rigeur* in BEC physics experiments. With the advent of lasers, they can be produced in a rather controlled manner. Can we then hope to see a superfluid state of light?

This is the question that I tried to answer over the course of this internship.

The problem with photons

Photons are simple to produce and experiment with, but they lack the important ingredient: interactions. Two photons are effectively transparent to each other. Photons without interactions have already been the subject of immense study ever since the Planck hypothesis. In fact, the photon gas was the first Bose gas ever studied in physics, and the question of a photon BEC is subject to exciting research conducted by Martin Weitz at Cologne [4]

So how do we make two photons interact with each other? We use matter as an intermediary between two photons. The presence of a non-linear medium showing a χ^3 non-linearity is a suitable candidate for the job. We shall explain the choice of a χ^3 material later in the report.

This heuristic definition might serve as a great tool for intuiting about photonic superfluidity. However, we do have a formal mathematical basis upon which to talk about the superfluid character of photons, which we shall demonstrate in a subsequent section.

The Quantum Optics team at LKB is already at the forefront in the research of polaritons, coupled states of excitons and photons in a microcavity, to study the phenomenon of superfluid light.

Presentation of the team

The Quantum Optics group at LKB works on two topics principally: nanofibers and quantum fluids of light. The study of quantum fluids of light is carried out via the study of polaritons generated in microcavities. The group, led by Alberto Bramati, has been able to demonstrate the superfluid aspects of light via a number of different criteria: the disappearance of turbulence as the fluid undergoes a superfluid transition and the presence of quantised vortices to name just a few examples [5], [6].

Thus, the current project is an extension of the study of quantum fluids of light via a different method: introducing interactions via a non-linear material. For this project, hot atomic vapor of an isotopic mixture of ^{85}Rb and ^{87}Rb was chosen as a non-linear material. The choice of Rubidium (Rb) vapor shall be discussed in a subsequent section.

Is light really superfluid?

When we mention that light shows superfluid character, we shall mean it in a rather specific context. This context shall be detailed over the course of the report. It is useful to look at this study from the viewpoint of quantum simulation.

The idea behind quantum simulation comes from Richard Feynman who suggested that rather than trying to simulate *in silico* many-body quantum systems, it would be better to find an analogous physical system which could *simulate* the real system. Today, the project of quantum simulation is a burgeoning one. We can now simulate in the lab anything from gauge fields to acoustic black holes [7], [8]

Thus the experiment conducted over the course of the internship has a dual purpose:

1. to possibly discover unseen effects of superfluidity
2. to provide a new set of tools and a new vocabulary for experimental physicists in quantum optics to study non-linear optics phenomena.

More generally, quantum simulation provides a physically meaningful way of finding analogies between physical systems which *a priori* don't seem to be related in any way. Furthermore, it leads to a high degree of cooperation between physicists of different domains.

Plan of the report

The report is structured in the following manner: we begin by a thorough theoretical discussion of the phenomena at hand. After a brief presentation of superfluidity, we present details of non-linear optical effects which are at the heart of the experiment. We finish our theoretical excursion by detailing out the analogy between *classical* superfluids and *optical* superfluids. The theoretical context having been established, we present the experimental details. We explain how we seek to demonstrate the superfluid character of light. Certain experimental techniques are presented. Non-linear media are rich because of the diversity of non-linear effects, such as self-defocussing and degenerate 4-wave mixing. These non-linear effects were present in the experiment and we discuss how we correct for them. We explain how we ascertained the relevant parameters of the experiment. In between the theoretical excursion and the experimental adventure, we digress to talk about the interplay between category theory and quantum simulation. Next, we present the experimental results, detailing the steps in data acquisition and data treatment. We conclude by resuming the results obtained and discuss possibilities of future experiments. Relevant technical details are to be found in the appendices.

Part II

Theoretical Background

We begin by giving an overview of the theoretical principles underlying the experiment. This section is planned as follows: we begin by describing the phenomenon that is superfluidity. We derive the Gross-Pitaevskii equation which describes the evolution of the wavefunction defining the superfluid state. We then present the derivation of the spectrum of weak excitation in a superfluid using the Boguliobov formalism.

In the next subsection, we present the required theoretical formalism of non-linear optics. We begin by presenting the two-level model. This model presents a simple way to understand resonant non-linearities of the kind that were used in our experiment. We then describe the propagation of light in a non-linear material. We also discuss the characteristics of such resonant non-linearities.

To end this section, we detail the analogy between the Gross-Pitaevskii equation (GPE) for superfluids and the Non-Linear Schrodinger equation for light propagation (NLSE). We discuss the analogous nature of various parameters in the two equations.

1 SUPERFLUIDITY IN CONDENSED MATTER PHYSICS

The phenomenon of superfluidity is a fascinating one. Discovered in 1937 in ^{4}He, it is one of the many macroscopic quantum phenomena that have been the subject of rigorous study over the past 50 years. The remarkable characteristics of superfluidity are zero viscosity beyond some critical temperature and the formation of quantized vortices. We shall not enter into the details of this singularly interesting phenomenon. We shall concentrate on some basic theoretical aspects concerning the dynamics of a superfluid.

1.1 Gross-Pitaevskii Equation

Superfluidity is a macroscopic quantum phenomena i.e. it is a many-body quantum effect. For such a system, the dynamics of the system are encoded in the wavefunction Ψ of the *whole* system, rather than any single particle. For superfluids and Bose-Einstein condensates, the dynamics are governed by the Gross-Pitaevskii equation, which is one example of the broader class of Non-Linear Schrodinger Equations.

$$i\hbar\frac{\partial}{\partial t}\Psi_0(r,t) = -\frac{\hbar^2\nabla^2}{2m}\Psi_0(r,t) + \mathrm{V}_{\mathrm{ext}}\Psi_0(r,t) + g|\Psi_0(r,t)|^2\Psi_0(r,t). \tag{1}$$

Here $\Psi_0(r,t)$ is the order parameter, g is the interaction constant governing the interaction between particles in the system, and $\mathrm{V}_{\mathrm{ext}}$ is the external potenial. The order parameter is a term reserved for the quantity that undergoes a phase transition in condensed matter physics. Using the Gross-Pitaevskii equation, we can understand a whole host of effects such as quantized vortices, formation of solitons and the creation of second sound [9]

1.2 Boguliobov Excitations

For what concerns this project, we shall concentrate not on the complex dynamics of the GPE, but on probing the small amplitude excitations present in a superfluid. Our eventual aim is to discover the dispersion relation which governs these excitations.

To start off, we can write these low amplitude excitations as a small perturbation on top of the superfluid state:

$$\Psi_0(r,t) = \left[\Psi_0(r) + \theta(r,t)\right] \mathrm{e}^{-i\mu t/\hbar}. \tag{2}$$

where μ is the chemical potential of the superfluid.

For $\theta(r,t)$, we are interested in solutions which take the form:

$$\theta(r,t) = \sum_i \left[u_i(r)\mathrm{e}^{-i\omega_i t} + v_i^* \mathrm{e}^{i\omega_i t}\right]. \tag{3}$$

We can inject this particular form of $\theta(r,t)$ into the GPE. Solving for u_i and v_i will then provide us the eigenfrequencies of the the normal modes of the system. In general, such solutions require numerical techniques. An analytic solution can be obtained by searching for elementary excitations around the ground state of the gas, i.e. $\mathrm{V}_{\mathrm{ext}} = 0$. Under this assumption, we find that Ψ_0 is inderpendent of $\mathbf{r}$ and $\mu = gn$. Ψ_0 can then be chosen to be real and we take $\Psi_0 = \sqrt{n}$. We thus find that $u(r)$, $v(r)$ are of the form $u(r) = u\mathrm{e}^{ikr}$, $v(r) = v\mathrm{e}^{ikr}$.

We then obtain a set of coupled equations

$$\hbar\omega u = \frac{\hbar^2 k^2}{2m} u + gn(u+v), \tag{4a}$$

$$-\hbar\omega v = \frac{\hbar^2 k^2}{2m} v + gn(u+v), \tag{4b}$$

which upon solving gives:

$$\boxed{(\hbar\omega)^2 = \left(\frac{\hbar^2 k^2}{2m}\right)^2 + \frac{\hbar^2 k^2}{m} gn.} \tag{5}$$

This is the famous Boguliobov dispersion relation for elementary excitations in a superfluid. The Boguliobov dispersion relation is characterized by the presence of two different regimes

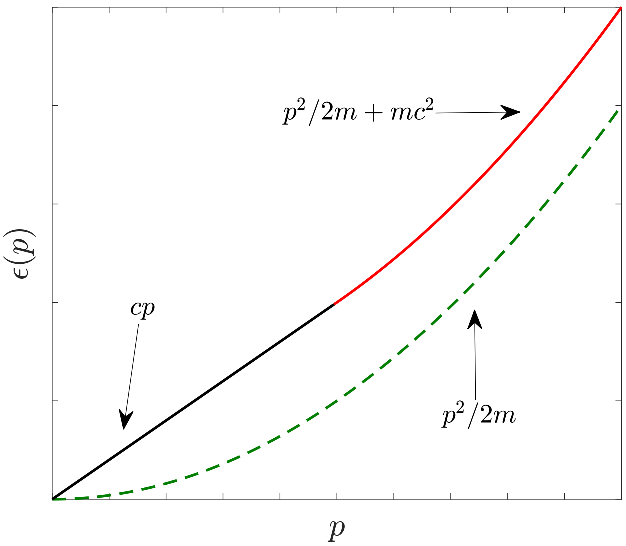

Figure 1: The Boguliobov dispersion relation for elementary excitations of a superfluid. There are two regimes: the linear phononic dispersion (shown in black) and the quadratic dispersion in red. The single particle dispersion is different from the standard dispersion relation (shown in dashed green) with the added term mc^2.

1. **Linear Dispersion**: For small momenta i.e. $\hbar k \ll mc$, with $c = \sqrt{gn/m}$, we have the relation

$$\hbar\omega = \hbar kc = \hbar k\sqrt{gn/m}, \tag{6a}$$

$$\epsilon(p) = cp. \tag{6b}$$

   We thus see that long wavelength excitations of the fluid are sound waves. Thus these excitations are phononic in nature.

2. **Quadratic Dispersion**: For large momenta i.e $\hbar k \gg mc$, we have the free particle dispersion relation

$$\hbar\omega = \frac{\hbar^2 k^2}{2m} + gn, \tag{7a}$$

$$\epsilon(p) = \frac{p^2}{2m} + mc^2. \tag{7b}$$

The transition between these two regimes takes place when $\hbar k \sim mc$. By writing $p = \frac{\hbar}{\xi}$, we can define a characteristic interaction length in the system as:

$$\xi = \sqrt{\frac{\hbar^2}{2mgn}} = \frac{1}{\sqrt{2}}\frac{\hbar}{mc}. \tag{8}$$

.

We remark also that ξ is the length scale at which the kinetic energy

$$\frac{p^2}{2m} = \frac{\hbar^2}{\xi^2} = mc^2. \tag{9}$$

Having considered the basic concepts underlying the dynamics of a superfluid, we now turn to the propagation of light and unravel the analogy with what we have just seen.

2
NON-LINEAR OPTICS

Let us begin with a simple working definition for non-linear optics phenomena. Non-linear optics can be thought of the study of phenomena in which the optical parameters of the system like the refractive index and polarization depend non-linearly on the electric field. This leads to phenomena like second harmonic generation, three-wave and four-wave mixing and self-focusing.

For what concerns us, we shall concentrate on the non-linear behavior of the refractive index.

2.1 Propagation of light in non-linear material

In the absence of sources, the equation of propagation of light is given by:

$$\nabla^2 E - \mu_0 \epsilon \frac{\partial^2 E}{\partial t^2} = 0, \epsilon = \epsilon(x, y, z), \tag{10}$$

where ϵ and μ_0 are the permittivity and permeability of respectively. Here ϵ is assumed to be a spatially varying function. We consider a particular class of electric fields E which propagate along the z-axis and envelope itself is assumed to be complex. Thus,

$$E(x, y, z, t) = E_e(x, y, z) \mathrm{e}^{i(\omega_0 t - k_0 z)}, \tag{11}$$

where E_e denotes the envelope of the electric field.

We then inject this form for the electric field into (10) to get

$$\nabla_\perp^2 E_e + \frac{\partial^2 E_e}{\partial z^2} - 2ik_0 \frac{\partial E_e}{\partial z} - (k_0^2 - \mu_0 \epsilon \omega_0^2) E_e = 0. \tag{12}$$

where $\nabla_\perp^2$ denotes the laplacian taken in the $x-y$ plane, i.e. plane transverse to the axis of propagation. We now make the paraxial approximation : we assume that E_e is a slowly varying function of z such that

$$\left| \frac{\partial E_e}{\partial z} \right| \ll k_0 E_e \text{ and } \left| \frac{\partial^2 E_e}{\partial z^2} \right| \ll k_0 \left| \frac{\partial E_e}{\partial z} \right|, \tag{13}$$

implying that within one wavelength of the propagation distance along the z-axis, the change in E_e is much smaller than the electric field itself. This leads to some simplification in (12). We then get

$$\nabla_\perp^2 E_e - 2ik_0 \frac{\partial E_e}{\partial z} - (k_0^2 - \mu_0 \epsilon \omega_0^2) E_e = 0. \tag{14}$$

This equation is known as the *Helmholtz Equation* in optics [10]. We now write the term $\mu_0\epsilon\omega_0^2$ in the following manner:

$$\mu_0\epsilon\omega_0^2 = \mu_0\epsilon_0\epsilon_r(1+\Delta\epsilon)\omega_0^2 = k_0^2 + k_0^2\Delta\epsilon, \tag{15a}$$
$$k_0^2 - \mu_0\epsilon\omega_0^2 = -k_0^2\Delta\epsilon, \tag{15b}$$

where ϵ_r is the relative permittivity and we have assumed that there is some small contribution to ϵ_r through its dependence on the electric field. $\Delta\epsilon$ is itself a function of the transverse coordinates $\Delta\epsilon = \Delta\epsilon(x,y)$ Through ϵ_r, we can now extract the expression for the refractive index n.

$$n(x,y) = n_0(1+\Delta n(x,y)) = \sqrt{\epsilon_r(1+\Delta\epsilon)} \tag{16a}$$
$$\approx \sqrt{\epsilon_r} + \frac{\sqrt{\epsilon_r}}{2}\Delta\epsilon, \tag{16b}$$
$$-k_0^2\Delta\epsilon = -2k_0^2\Delta n. \tag{16c}$$

Putting the pieces together, we get the following equation, known as the paraxial propagation equation. It is also known as the *Non-linear Schrodinger equation for Light.* The significance of this nomenclature will become clearer in subsequent sections.

$$\boxed{\frac{\partial E}{\partial z} = \frac{i}{2k}\nabla_\perp^2 E - ik\Delta n E.} \tag{17}$$

The refractive index n can then be written as the sum of two terms: a linear term which is independent of the incident electric field, and a non-linear term which characterizes the dependence on the electric field. Thus, the refractive index n can then be written as :

$$n = n_0 + n_2 f(E). \tag{18}$$

We shall elucidate the $f(E)$ in the subsequent sections. n_2 is usually called second-order index of refraction. In simple terms n_2 gives the rate at which the refractive index changes with respect to a change in the incident electric field.

2.2 Non-linear refractive index

The interaction of a non-linear material with an incident beam of light can be described in terms of the non-linear polarizations. Polarization **P** describes how a material responds to an applied electric field on the one hand, and the way the material influences the electric field. The response of the system to a change in the electric field can be quantified via a quantity known as the susceptibility. In more general terms, if we consider a change in the electric field as a fluctuation and the subsequent change in the polarization as a response to the fluctuation, then the susceptibility written as χ gives the coupling between the fluctuation and the response i.e.

$$\mathbf{P} = \epsilon_0 \chi \mathbf{E}. \tag{19}$$

The susceptibility χ is related to the permittivity via the Clausius-Mosotti relation. We can write :

$$\chi = \epsilon_r - 1. \tag{20}$$

We can now give a more precise definition of what constitutes a non-linear material: a non-linear material is such that the susceptibility χ is not a constant (or some trivial linear mapping between $\mathbf{P}$ and $\mathbf{E}$). In general, we can write the polarization as a Taylor expansion in the electric field as:

$$P = P_0 + \epsilon_0 \chi^{(1)} E + \epsilon_0 \chi^{(2)} E^2 + \epsilon_0 \chi^{(3)} E^3 + \cdots \tag{21}$$

Here $\chi^{(1)}$ is known as the linear susceptibility (the kinds we are accustomed to in standard courses in electromagnetism). Higher order terms are known as second-order, third-order or n-order susceptibilities. For isotropic mediums, the susceptibility terms are complex numbers. However, for anisotropic materials, the higher order susceptibilities are usually $(n-1)$-order rank tensors. This tensorial character takes into the account the fact that a change in the electric field in a particular direction can engender a response in a different direction. Thus, in general χ is a tensor.

For centro-symmetric materials, there is no second-order susceptibility term [10][11].

Centro-symmetric materials

For centrosymmetric materials, we can write the polarization as :

$$P : (x, y, z) \to (-x, -y, -z). \tag{22}$$

Suppose that the polarization of such a material can be written as :

$$P_i = A_{ij} E_j + B_{ijk} E_{jk}. \tag{23}$$

Under the transformation (22), we get that (since $\mathbf{P}$ and $\mathbf{E}$ are vectors)

$$P_i \to -P_i, \qquad E_i \to -E_i. \tag{24}$$

For centrosymmetric crystals, the constants A, B are constant under the transformation (22).

$$A_{ij} \to A_{ij}, \qquad B_{ijk} \to B_{ijk}. \tag{25}$$

It is important to note that there is no sign change for B. In other terms, under a centrosymmetric transformation, we get back the same material and the material constants, including tensorial quantities such as B remain the same.

Finally, when we apply the transformation (22) to the polarization, we get

$$-P_i = -A_{ij}E_j + B_{ijk}E_jE_k. \tag{26}$$

Thus, the only way in which (24) can be satisfied is if $B = 0$. We conclude that only odd powers of E can be present in the expression for non-linear polarization. Thus the lowest non-linear term for the polarization is cubic in E.

We can thus write the non-linear polarization as

$$P^{\text{NL}}(\omega) = 3\epsilon_0\chi^{(3)}(\omega)|E(\omega)|^2E(\omega), \tag{27}$$

where the factor 3 comes about by taking into account the various effects such as sum-frequency and difference-frequency generation [11].

Thus the total polarization P is given by

$$P^{\text{TOT}} = \epsilon_0\chi^{(1)}E(\omega) + 3\epsilon_0\chi^{(3)}|E(\omega)|^2E(\omega) \equiv \epsilon_0\chi_{\text{eff}}E(\omega), \tag{28}$$

where $\chi_{\text{eff}} = \chi^{(1)} + 3\epsilon_0\chi^{(3)}|E(\omega)|^2$. We can now write the function $f(E)$ that was left unstated in (18).

$$n^2 = \epsilon_r = \chi_{\text{eff}}. \tag{29}$$

Writing the $f(E)$ in terms of the time averaged value of the electric field and assuming $f(E)$ to be linear in E we get that

$$f(E) = f(\langle E\rangle) = f(2|E(\omega)|^2) = 2f(|E(\omega)|^2). \tag{30}$$

We find thus

$$[n_0 + 2f(|E(\omega)|^2)]^2 = 1 + \chi^{(1)} + 3\epsilon_0\chi^{(3)}|E(\omega)|^2, \tag{31a}$$
$$n_0^2 + 4n_0n_2f(|E(\omega)|^2) = (1 + \chi^{(1)}) + 3\epsilon_0\chi^{(3)}|E(\omega)|^2. \tag{31b}$$

We thus identify that $f(|E(\omega)|^2) = |E(\omega)|^2$. Finally, we derive the relations between the susceptibilities and the refractive indices as:

$$\boxed{\begin{aligned} n_0 &= \sqrt{1+\chi^{(1)}}, && (32)\\ n_2 &= \frac{3\chi^{(3)}}{4n_0}. && (33)\end{aligned}}$$

Usually in optics experiments, we measure not the amplitude of the electric fields themselves but the intensity of the incident light. Here the intensity is defined as the average power per unit area. The intensity denoted by I can be written in terms of the electric field as

$$I = 2n_0\epsilon_0 c|E(\omega)|^2. \tag{34}$$

We thus write $n = n_0 + n_2 I$, where n_0 and n_2 are written as:

$$\boxed{\begin{aligned} n_0 &= \sqrt{1+\chi^{(1)}}, && (35)\\ n_2 &= \frac{3\chi^{(3)}}{4n_0^2\epsilon_0 c}. && (36)\end{aligned}}$$

2.3 Resonant non-linearities

After having established the theoretical basis for the non-linear refractive index, we shall consider non-linearities in an atomic medium. Such non-linearities are generated by the interaction of an incident electric field which is slightly detuned from an atomic resonance. Since the experiment was conducted with an atomic vapor as a non-linear medium, we will give a complete theoretical description of the such non-linearities.

2.3.1 • Two-level model

We begin with a very simple but powerful model to describe the interaction between atoms and light: the two-level atom. As Bill Phillips has said

There are no two-level atoms, and rubidium is not one of them

it is a valid model to understand atom-light interactions when the incident light is not highly detuned from resonance.

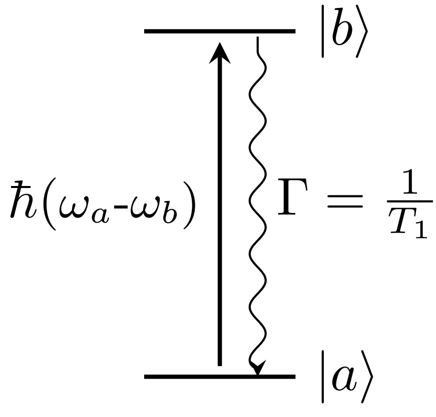

Figure 2: Two level atom showing transition between states $|a\rangle$ and $|b\rangle$. The difference in energy between the two levels is $\hbar(\omega_a - \omega_b)$. The state $|b\rangle$ decays into the state $|a\rangle$ with decay constant Γ.

We take a two level atomic system with states $|a\rangle$ and $|b\rangle$. We shall denote the energy difference between these two levels as $\hbar(\omega_b - \omega_a)$. We also allow the level $|b\rangle$ to decay into the level $|a\rangle$ in some characteristic time T_1 or at the rate $\Gamma_{ba} = \frac{1}{T_1}$. Furthermore, the system is assumed to be closed i.e. the level $|b\rangle$ is not allowed to decay into some other level.

The interaction with the external electric field is $V(t)$, which written in the Coulomb gauge is the product of a quantum mechanical dipole operator $\hat{\mu}$ and the electric field $\tilde{E}$ taken to be complex.

$$\hat{V} = -\hat{\mu}\tilde{E}(t) = -\hat{\mu}(E\mathrm{e}^{-i\omega t} + E^*\mathrm{e}^{i\omega t}), \tag{37}$$

$$V_{ba} = -\mu_{ba}(E\mathrm{e}^{-i\omega t} + E^*\mathrm{e}^{i\omega t}). \tag{38}$$

The dynamics of such a two level system are expressed in terms of the density matrix for the system.

$$\hat{\rho} = \begin{bmatrix} \rho_{aa} & \rho_{ab} \\ \rho_{ba} & \rho_{bb} \end{bmatrix}. \tag{39}$$

The evolution of the density matrix can be written in terms of the Heisenberg equation.

$$i\hbar\frac{\mathrm{d}\hat{\rho}}{\mathrm{d}t} = -\left[\hat{\rho}, \hat{H}\right], \tag{40}$$

where $\hat{H} = \hat{H}_0 + \hat{V}$:

$$\hat{H} = \begin{bmatrix} \hbar\omega_a & V_{ab} \\ V_{ba} & \hbar\omega_b \end{bmatrix}. \tag{41}$$

From (40), we get:

$$\frac{\mathrm{d}\rho_{ij}}{\mathrm{d}t} = -\frac{i}{\hbar}\left[\hat{H}, \hat{\rho}\right]_{ij} = -\frac{i}{\hbar}\sum_k (H_{ik}\rho_{kj} - \rho_{ik}H_{kj}). \tag{42}$$

We write the transition frequency between the states $|a\rangle$ and $|b\rangle$ as ω_{ab}. Using (37), we get for each of the terms in the density matrix:

$$\dot{\rho}_{ba} = -i(\omega_{ba}\rho_{ba}) + \frac{i}{\hbar}\mathrm{V}_{ba}(\rho_{bb} - \rho_{aa}), \tag{43a}$$

$$\dot{\rho}_{bb} = \frac{i}{\hbar}(\mathrm{V}_{ba}\rho_{ab} - \rho_{ba}\mathrm{V}_{ab}), \tag{43b}$$

$$\dot{\rho}_{aa} = \frac{i}{\hbar}(\mathrm{V}_{ab}\rho_{ba} - \rho_{ab}\mathrm{V}_{ba}). \tag{43c}$$

We observe that $\dot{\rho}_{bb} + \dot{\rho}_{aa} = 0$ implying that

$$\rho_{aa} + \rho_{bb} = 1, \tag{44}$$

since the diagonal elements of $\hat{\rho}$ represent occupation probabilities of states $|a\rangle$ and $|b\rangle$. Furthermore, since $\hat{\rho}$ is hermitian, $\rho_{ab} = \rho_{ba}^*$, we need only write the equation for ρ_{ba}.

The solution of (43) provide a complete description of a two-level system without any relaxation processes. However, for a two level system which can spontaneously decay from $|b\rangle$ to $|b\rangle$, we need to add relaxation terms to these equations. This is done phenomenogically by adding relaxation terms proportional to the decay constant Γ_{ba}. We obtain thus,

$$\frac{\mathrm{d}}{\mathrm{dt}}(\rho_{bb} - \rho_{aa}) = -\Gamma_{ba}(\rho_{bb} - \rho_{aa} + 1) - \frac{2i}{\hbar}(\mathrm{V}_{ba}\rho_{ab} - \rho_{ba}\mathrm{V}_{ab}), \tag{45a}$$

$$\frac{\mathrm{d}}{\mathrm{dt}}\rho_{ba} = -(i\omega_{ab} + \frac{\Gamma_{ba}}{2})\rho_{ba} + \frac{i}{\hbar}\mathrm{V}_{ba}(\rho_{bb} - \rho_{aa}), \tag{45b}$$

where we write one equation for the population difference $\rho_{bb} - \rho_{aa}$.

In general, equations (45) are not solvable. We thus make the rotating-wave approximation such that (37) as [11]

$$V_{ba} = -\mu_{ba}E\mathrm{e}^{-i\omega t}. \tag{46}$$

Under this approximation the density matrix equations become

$$\frac{\mathrm{d}}{\mathrm{d}t}\rho_{ba} = -\left(i\omega_{ba} + \frac{\Gamma_{ba}}{2}\right)\rho_{ba} + \frac{i}{\hbar}\mu_{ba}E\mathrm{e}^{-i\omega t}(\rho_{bb} - \rho_{aa}), \tag{47a}$$

$$\frac{\mathrm{d}}{\mathrm{d}t}(\rho_{bb} - \rho_{aa}) = -\Gamma_{ba}(\rho_{bb} - \rho_{aa} + 1) + \frac{2i}{\hbar}(\mu_{ba}E\mathrm{e}^{-i\omega t}\rho_{ab} - \mu_{ab}E^*\mathrm{e}^{i\omega t}\rho_{ba}). \tag{47b}$$

In steady-state, with the condition $\rho_{aa} + \rho_{bb} = 1$, the solutions to (47) are

$$\rho_{bb} - \rho_{aa} = -\frac{1 + \left[(\omega - \omega_{ba})\Gamma_{ba}^2/4\right]}{1 + (\omega - \omega_{ba})^2\frac{\Gamma_{ba}^2}{4} + \frac{2}{\hbar^2}|\mu_{ba}|^2|E|^2\Gamma_{ba}^2}, \tag{48}$$

$$\rho_{ba} = \frac{\mu_{ba}E\mathrm{e}^{i\omega t}(\rho_{bb} - \rho_{aa})}{\hbar(\omega - \omega_{ba} + \frac{i\Gamma_{ba}}{2})}. \tag{49}$$

2.3.2 • Susceptibility

Using the solutions (48), we can now define and calculate the polarization which is defined as the dipole moment per unit volume. Using the dipole moment operator $\hat{\mu}$, we have

$$\tilde{P}(t) = N\langle\mu\rangle = N(\mu_{ab}\rho_{ba} + \mu_{ba}\rho_{ab}). \tag{50}$$

where N is the number of density of atoms.

From (19), we get for the susceptibility

$$\chi = \frac{N|\mu_{ba}|^2(\rho_{bb} - \rho_{aa})}{\epsilon_0 \hbar(\omega - \omega_{ba} + i\Gamma_{ba}/2)}. \tag{51}$$

Injecting the solution for $(\rho_{bb} - \rho_{aa})$ from (48), we get,

$$\chi = -\frac{N|\mu_{ba}|^2(\omega - \omega_{ba} - i\Gamma_{ba}/2)\frac{\Gamma_{ba}^2}{4\epsilon_0\hbar}}{1 + (\omega - \omega_{ba})^2\Gamma_{ba}^2/4 + \frac{2\Gamma_{ba}^2}{\hbar^2}|\mu_{ba}|^2|E|^2}. \tag{52}$$

To make the expression more compact, we introduce the terms

1. $\delta = \omega - \omega_{ba}$, which denotes the detuning
2. $\Omega_R = |\mu_{ba}||E|/\hbar$, which denotes the Rabi frequency of the two level system
3. $\Gamma = \Gamma_{ba}$, which denotes the relaxation rate from state $|b\rangle$ to $|a\rangle$

With this notation and after some simplification we get for χ

$$\chi = \left[-4N|\mu_{ba}|\frac{\Omega_R}{E\epsilon_0\Gamma^2}\right]\frac{\delta - i\Gamma/2}{1 + \frac{4\delta^2}{\Gamma^2} + \frac{8\Omega_R^2}{\Gamma^2}}. \tag{53}$$

To be able to extract the non-linear refractive index from this expression for χ, we will perform an expansion of (53) in $|E|^2$. To this end, we make the following substitutions:

$$C = \left[-4N|\mu_{ba}|\frac{\Omega_R}{E\epsilon_0\Gamma^2}\right], \tag{54a}$$

$$\frac{8\Omega_R^2}{\Gamma^2} = \frac{|E|^2}{|E_s|^2}, \tag{54b}$$

$$|E_s|^2 = \frac{\Gamma^2\hbar^2}{8|\mu_{ba}|^2}. \tag{54c}$$

We then have for χ,

$$\chi = C\left(\frac{\delta - i\Gamma/2}{1 + \frac{4\delta^2}{\Gamma^2} + \frac{|E|^2}{|E_s|^2}}\right). \tag{55}$$

A small comment on the significance of the term $|E_s|^2$: We observe from the expression that for an optical field of $|E_s|^2$, the value of the susceptibility falls to half its maximum value.

We now perform a Taylor expansion in $|E|^2/|E_s|^2$, to get

$$\chi = C\left(\frac{\delta - i\Gamma/2}{1 + \frac{4\delta^2}{\Gamma^2}}\right)\left(1 - \frac{1}{1 + \frac{4\delta^2}{\Gamma^2}}\frac{|E|^2}{|E_s|^2}\right). \tag{56}$$

We now identify the first-order and third-order susceptibility, from the above expression

$$\chi^{(1)} = C\left(\frac{\delta - i\Gamma/2}{1+\frac{4\delta^2}{\Gamma^2}}\right), \tag{57a}$$

$$\chi^{(3)} = \frac{C}{3}\frac{(\delta - i\Gamma/2)}{(1+\frac{4\delta^2}{\Gamma^2})^2}\frac{1}{|E_s|^2}. \tag{57b}$$

Since we are concerned with the non-linear refractive index, we shall concentrate on the expression for $\chi^{(3)}$. Replacing the value of $|E_s|^2$ above and rearranging the terms, we get

$$\chi^{(3)} = \frac{32N\mu_{ba}^4}{3\epsilon_0\hbar^3}\frac{\delta/\Gamma^4}{(1+\frac{4\delta^2}{\Gamma^2})^2}. \tag{58}$$

The real part of $\chi^{(3)}$ corresponds to the non-linear refractive index whilst the imaginary part corresponds to the absoprtion coefficient α. From (35), we get for n_2

$$\boxed{n_2 = \frac{8N\mu_{ba}^4}{\epsilon_0^2 c n_0^2\hbar^3}\frac{\delta/\Gamma^4}{(1+\frac{4\delta^2}{\Gamma^2})^2}.} \tag{59}$$

Furthermore, for highly detuned systems such that $\delta \gg \Gamma$, we have the expression:

$$\boxed{n_2 \approx \frac{N|\mu_{ba}|^4}{2\epsilon_0^2 n_0^2\hbar^3}\frac{1}{\delta^3}.} \tag{60}$$

We have thus been able to give a microscopic expression for the non-linear refractive index using a very simple model of the two-level system. We shall use this expression in what follows to better understand the atomic system that was used as well as calibrate the experiment performed to the optimal value of n_2.

Before we get into the experimental details, we shall spend some time on elucidating the relation between superfluidity and the propagation of light in a non-linear medium.

3
SUPERFLUIDITY OF LIGHT

Let us recapitulate the two equations which govern the dynamics of superfluids (without an external potential) on one hand and the propagation of light in a non-linear medium on the other hand.

$$i\hbar\frac{\partial}{\partial t}\Psi_0(r,t) = -\frac{\hbar^2\nabla^2}{2m}\Psi_0(r,t) + g|\Psi_0(r,t)|^2\Psi_0(r,t), \tag{61a}$$

$$\frac{\partial E}{\partial z} = \frac{i}{2k}\nabla_\perp^2 E - ikn_2|E|^2 E. \tag{61b}$$

We remark right away that these two equations are equivalent mathematically, even though they represent two different physical situations. The equivalence is complete if we identify the parameter t (time) for z, and the complete laplacian ∇^2 with the transverse laplacian $\nabla_\perp^2$. We then ask the rather legitimate question: if these two equations are equivalent (upto some transformations), will the systems they describe exhibit similar behavior?

The answer is affirmative. Let us recall the conditions required for the existence of superfluid behavior that we introduced in the introduction. There we had remarked that we require bosons in interaction as a requirement for superfluid phenomena. We observe for the propagation of light in a non-linear medium that these two conditions are met: photons are bosons and the presence of matter can serve as an intermediate for creating an effective interaction between photons. A consequence of this effective interaction is self-defocusing, whereby a focused beam of light expands and gets defocused as it propagates through a non-linear medium (with negative non-linearity i.e. $n_2 < 0$). We can thus imagine that the presence of matter enables the photons to interact in a repulsive manner. However, we could in fact tune the interaction to have attractive interactions between the photons. This change in regimes can be established by a judicious choice of the non-linear refractive index n_2.

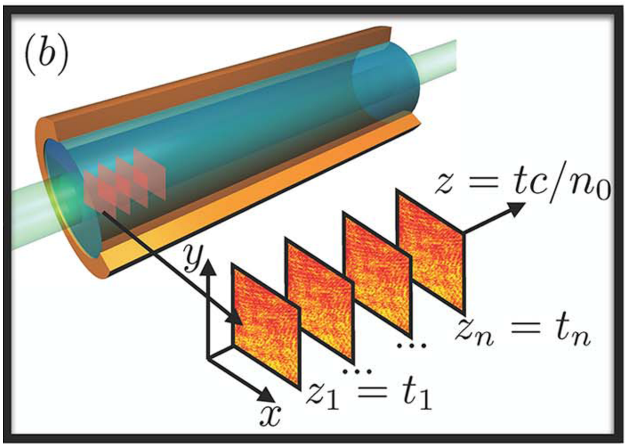

Figure 3: Time, in the GPE is mapped to the axis of propagation z for light. Every slice of the transverse plane at a given value of z can be regarded as corresponding to an instant of time t for the GPE. Taken from [12].

The equivalence between the two equations can be furthered established by an equivalence of parameters:

$$t \to \frac{z}{c}, \tag{62a}$$

$$v \to \frac{c}{k}\nabla\phi, \tag{62b}$$

$$\rho \to |E|^2, \tag{62c}$$

$$\xi \to \frac{\lambda}{2}\sqrt{\frac{1}{\Delta n}}, \tag{62d}$$

where v denotes the velocity of the fluid of light, $\nabla\phi$ is the phase of the electric field, and ξ is the healing length whose significance will become clearer in the next few sections.

Now that we have established the equivalence of the two systems: atomic superfluids with the dynamics governed by the GPE on the one hand, and the propagation of light in a non-linear light on the other, let us examine how we can experimentally verify the veracity of the equivalence, and in the process demonstrate the existence of a fluid of light.

Part III

Experimental Details

In this section of the report, we will examine how we can experimentally verify the existence of fluid of light in analogy with the propagation of light in a non-linear medium with that of atomic superfluids.

4
AIM OF THE EXPERIMENT

There are many methods to demonstrate the analogy between the flow of superfluids and the propagation of light in interesting geometries: at LKB, the quantum optics group has worked on a system called exciton polaritons. These polaritons are short-lived (of the order of picoseconds) quasi-particles created due to the interaction between photons and excitons in an optical cavity. There they have been able to demonstrate superfluidity and the existence of quantized vortices by the injection of angular momentum states in a polaritonic fluid of light [6].

The research on exciton polaritons is at an advanced stage. However, the aim of the experiments conducted over the course of this internship were different: demonstration of the superfluidity of light using atomic vapor as the non-linear medium. Since the work on atomic vapor as a potential source for creating superfluid-like behavior is at a nascent stage, we chose a simple method to demonstrate the unique properties of light in atomic vapor.

Thus, the aim of the experiment is to determine the spectrum of low-amplitude excitations in the quantum fluid of light. A straight-forward way to do this is via analogy with the GPE for atomic superfluids. We recall from (5) that the dispersion relation for low-amplitude elementary excitations is given by

$$(\hbar\omega)^2 = \left(\frac{\hbar^2 k^2}{2m}\right)^2 + \frac{\hbar^2 k^2}{m} gn. \tag{63}$$

By the same measure and using the equivalence of parameters established in (62), we find the dispersion relation for elementary excitations for the quantum fluid of light also follow the Boguliobov dispersion relation:

$$\Omega_\perp^2 = c^2 \Delta n K^2 + \frac{c^2}{4k^2} K^4, \tag{64}$$

where c is the speed of light in vacuum. $\Omega_\perp$ corresponds to the *spatial* frequency ($\Omega_\perp$ is written in terms of the temporal variable $t = \frac{z}{c}$) and K corresponds to the wave-vector. Both K and $\Omega_\perp$ correspond to quantities measured in the plane perpendicular to the propagation axis. We thus remark that similar to superfluids, two regimes exist corresponding to low and high momenta excitations: linear dispersion corresponding to phonon-like excitations and quadratic dispersion corresponding to single-particle like excitations.

We also define a few other terms: the transverse plane is the plane perpendicular to the propagation axis. All quantities with transverse prefixed before them correspond to the quantities measured in the transverse plane.

The method we use to probe the Boguliobov spectrum is the pump-probe technique

5 PUMP-PROBE TECHNIQUE

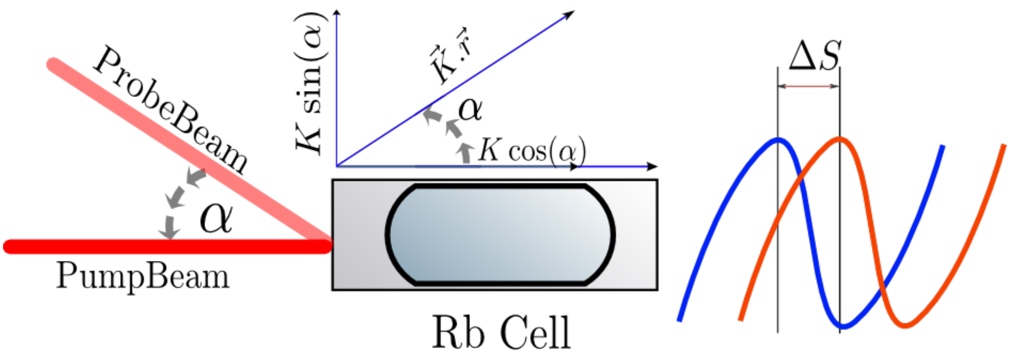

Figure 4: The pump-probe technique used in the experiment. The probe enters the incident face of the Rb *cell at an angle α. The transverse component is $K\sin(\alpha)$. At low intensities of the background field (the pump beam), we have very little non-linearity. The interference between the pump and probe beams under such conditions serves as a reference. When we* switch on *the non-linearity, the low-amplitude excitations propagate with a different phase velocity. This results in a shift between the reference interference pattern (in blue) and the non-linear interference pattern (in red).*

The pump-probe technique consists of creating a strong background fluid formed by an intense beam propagating along the z-axis. Then, another beam, weaker in intensity, is interfered with the pump beam. The probe beam enters the incident face of the medium at an angle α to the pump beam. This provides a propagation component of the probe beam in the transverse plane. Thus the interference between the pump and probe beam also has a transverse component which will serve as the low-amplitude excitation for the purposes of the experiment.

The angle between the pump and the probe provides us a way to modulate the transverse wave-vector K whilst the intensity of the background fluid provides us a means to modulate the interaction term and thus Δn.

However, the pump-probe technique in itself provides a way to create low amplitude excitations on top of the superfluid. We require another physical and measurable quantity to establish the superfluid nature of light.

To compute this quantity, we observe that the propagation of low-amplitude excitations would be different if the pump intensity was changed. Because the dispersion relation for the case where the pump has low intensity and one where it has high intensity (64) are different, this difference will be manifested in a shift in the interference pattern created by the pump and the probe beams in the two regimes.

This shift can be calculated by a simple calculation. The shift is a consequence of the difference in the phase velocity due to the differences in regimes depending on whether the pump has a high or low intensity. We remark that due to the $t \to z$ correspondence, the phase velocity which we note as v_{ph} is dimensionless. We can calculate the phase velocity from the dispersion by :

$$v_{ph} = \frac{\Omega_\perp}{cK} \tag{65}$$

The dispersion relation, and the phase velocity, when the pump has low intensity is given by

$$\Omega_\perp^{\mathrm{LP}} = \frac{c}{2k}K^2, \tag{66a}$$
$$v_{ph}^{\mathrm{LP}} = \frac{K}{2k}, \tag{66b}$$

where LP stands for Low-power. We note that in the low power case, $\Delta n = n_2 I$ is very small and we can safely neglect the term with Δn in the Boguliobov relation. For the high power case, which we note by HP, we have

$$\Omega_\perp^{\mathrm{HP}} = \sqrt{c^2 \Delta n K^2 + \frac{c^2}{4k^2}K^4}, \tag{67a}$$
$$v_{ph}^{\mathrm{HP}} = \frac{K}{2k}\sqrt{1 + \Delta n \left(\frac{2k}{K}\right)^2}, \tag{67b}$$

The shift can now be understood as the difference in *distance* covered by the low-amplitude excitations due to the difference in phase velocities of the background fluids. This retard, or shift, can be calculated by computing the difference in *distance* covered for the same amount of time. For our case, the time is in fact z, the distance along the propagation axis. Hence, the shift can be calculated as:

$$\Delta S = (v_{ph}^{\mathrm{HP}} - v_{ph}^{\mathrm{LP}})z. \tag{68}$$

Injecting the expressions for the phase velocities in the high power and low power regimes, we get

$$\boxed{\Delta S = \frac{Kz}{2k}\left[\sqrt{1 + \Delta n \left(\frac{2k}{K}\right)^2} - 1\right].} \tag{69}$$

In terms of Λ, the equation for the shift is:

$$\boxed{\Delta S = \frac{\lambda}{2\Lambda}\left[\sqrt{1+\Delta n\left(\frac{2\Lambda}{\lambda}\right)^2}-1\right]} \tag{70}$$

The shift ΔS as a function of $\Lambda = \frac{2\pi}{K}$ is shown in figure 5

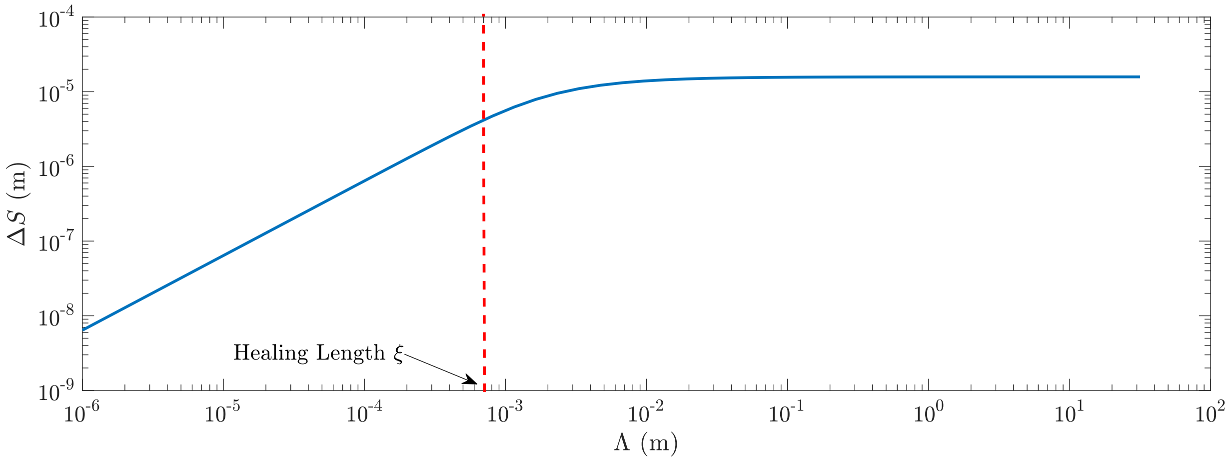

Figure 5: The variation of the shift ΔS with Λ for a non-linear medium. We identify also the healing length $\xi = 7\times 10^{-4}m$.

In the graph we see that beyond the healing length, there is a change in the regime of the shift, and the shift seems to saturate for higher values of Λ (or lower values of K). Thus for large values of Λ, we are in the phononic dispersion regime. Since the shift ΔS serves as a proxy for the dispersion relation for elementary excitations on top of the fluid, establishing the ΔS vs Λ curve is akin to getting information about the dispersion relation. Furthermore, by repeating the above calculation in reverse, we can get back the dispersion relation from the shift.

Having discussed the aim of the experiment, let us now discuss some features of the experiment.

6
DETERMINATION OF PARAMETERS

The experiment aims to demonstrate the analogy between the propagation of light in a non-linear medium and atomic superfluidity. What sets this experiment apart from other approaches such as the experiments with polaritons is that the experiment is conducted at room temperature. In other systems such as exciton polaritons, sophisticated cooling techniques are required to perform the experiment.

The non-linear material chosen for the purposes of the experiment is Rb vapor at a high temperature usually $140° - 150°$ celsius. The Rb is present in its naturally abundant form i.e. as an isotopic mixture of ^{85}Rb and ^{87}Rb.

Finally, we need to fix certain parameters of the experiment. From the expression of the shift (69), we see that we see that we have two free parameters: Δn and z, the propagation length. We chose a Rb cell with a length of 15cm and thus for the course of the experiment, $z = 15$cm. Δn on the other hand depends on some other parameters

1. Two level system, which determines the reference for the detuning δ
2. Intensity I of the laser beam.

While the two-level system will fix the value of n_2, we can scale the non-linearity Δn by varying I. For the two-level system, we choose the atomic resonance corresponding to $F = 2 \rightarrow F = 3$ hyperfine transition of the ^{87}Rb D_2 line. The transition is marked in red in figure 6. Having fixed the two-level system, we will discuss how we can determine Δn for this atomic system.

6.1 n_2

We have already calculated the expression for n_2 as a function of the detuning parameter in (59). However, n_2 depends on other factors, some of which are implicit and some of which are explicit. We rewrite the expression for n_2 for reference:

$$n_2 = \frac{8N\mu_{ba}^4}{\epsilon_0^2 c n_0^2 \hbar^3} \frac{\delta/\Gamma^4}{(1 + \frac{4\delta^2}{\Gamma^2})^2}. \tag{71}$$

In this expression, $n_2 \propto N$, the atomic density. The atomic density in turn is a function of the temperature T of the atomic vapor. The temperature dependence is important not just for the atomic density but for the detuning δ as well through the Doppler Effect. We know that at some temperature T, atomic velocities are distributed according to the Maxwell-Boltzmann distribution given by

$$\begin{aligned} W(v) &= \sqrt{\frac{m}{2\pi k_B T}} \mathrm{e}^{-\frac{v^2}{2a^2}}, \\ a &= \sqrt{\frac{k_B T}{m}}, \end{aligned} \tag{72}$$

where k_B is Boltzmann's constant. Thus for an atom moving along the axis of propagation at a speed v, the detuning observed for this atom would be

$$\delta_v = \delta - kv, \tag{73}$$

where $k = \frac{2\pi}{\lambda}$ is the wave-vector for the incident light. Thus, for an atomic system at temperature T, n_2 includes contributions from all velocity classes. We thus need to sum over all velocity classes i.e.

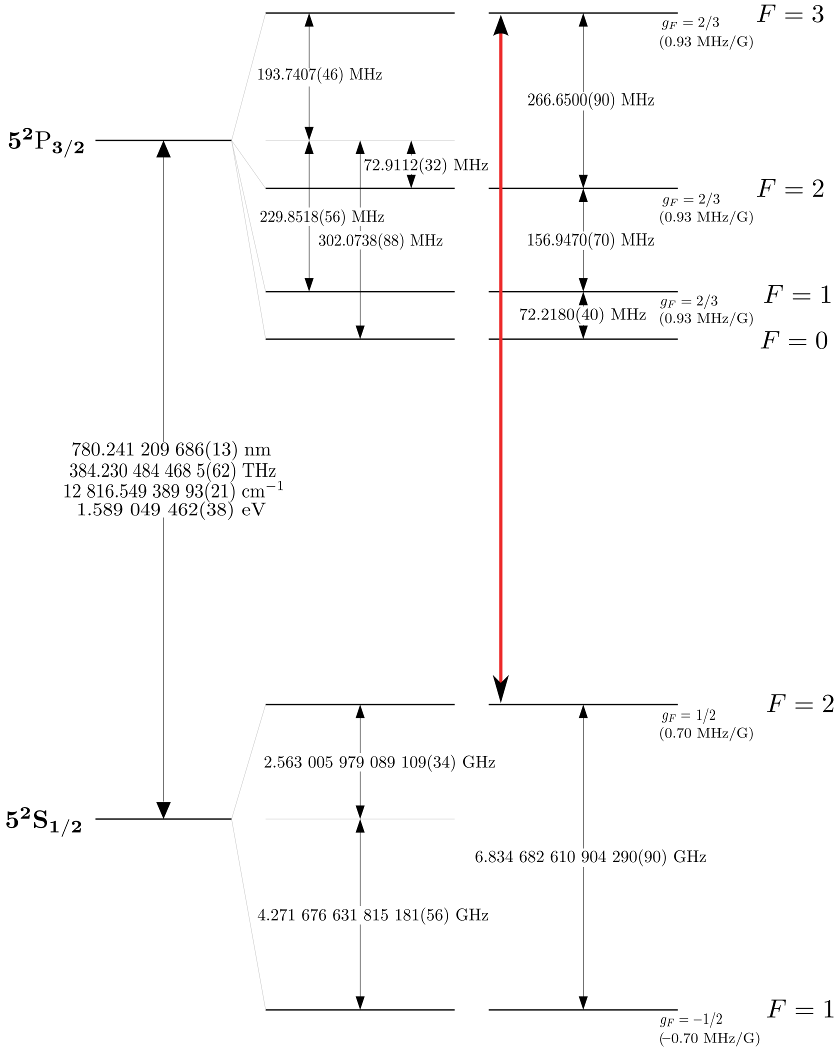

Figure 6: Hyperfine structure of ^{87}Rb *for the* D_2 *line corresponding to* $5^2\mathrm{S}_{1/2} \to 5^2\mathrm{P}_{3/2}$ *transition.*

$$n_2(v,T) = \frac{8N(T)\mu_{ba}^4}{\epsilon_0^2 c n_0^2 \hbar^3} \frac{\delta_v/\Gamma^4}{(1+\frac{4\delta_v^2}{\Gamma^2})^2}, \tag{74a}$$

$$n_2(T) = \int n_2(v,T)W(v)dv. \tag{74b}$$

This integral is computed numerically. We present the variation of Δn as a function of the detuning δ summed over all velocity classes.

However, we remark that the curve isn't nullified at $\delta = 0$ but in fact at $\delta \approx 1$GHz. This can be explained by taking into account the contribution of the ^{85}Rb isotope. In effect, we remark that there

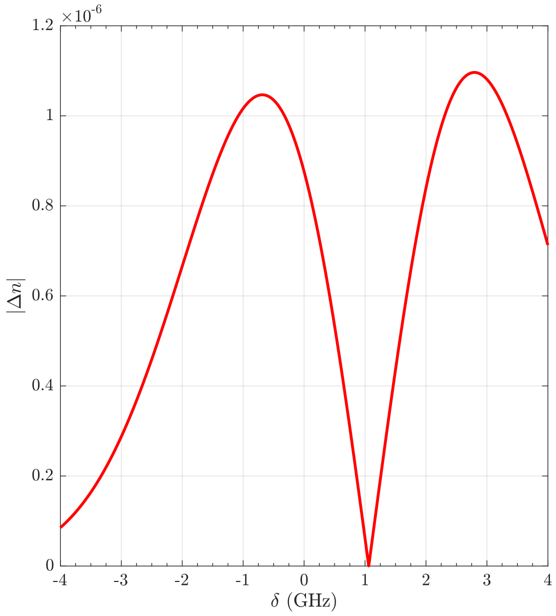

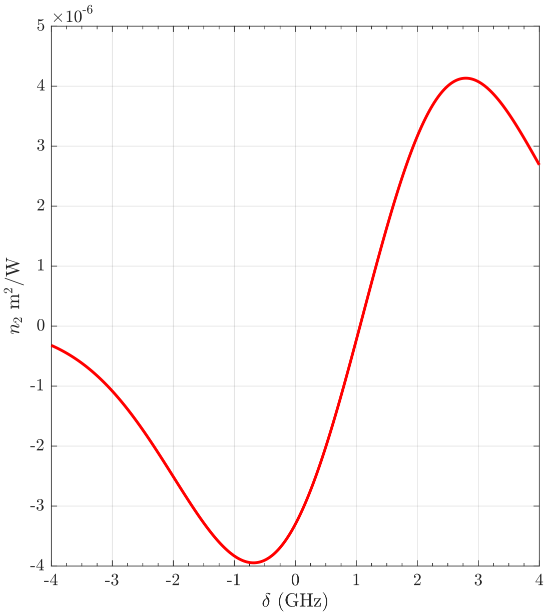

*Figure 7: **Left**: $|\Delta n|$ is plotted as a function of δ. The temperature was $142.5°$ Celsius with a beam size of 6 mm^2 and incident power of 50mW. **Right**: The variation of n_2 as a function of δ. The curve is an odd function of δ and for $\delta \gg 1$, it falls off as $1/\delta^3$.*

is non-negligible contribution from the 85-isotope as shown in figure 8 Furthermore, we remark that when we sum these two contributions, they nullify each other at $\delta \approx 1$GHz. We thus observe that even though our line center corresponds to the 87-isotope, we still have contributions from the 85-isotope. Moreover, since the number of 85-isotope is about 3 times as much as the 87-isotope, the contribution from the 85-isotope helps to increase the non-linear refractive index especially for $\delta < 0$. This is crucial since we require a regime in which $n_2 < 0$ for repulsive interactions between the photons.

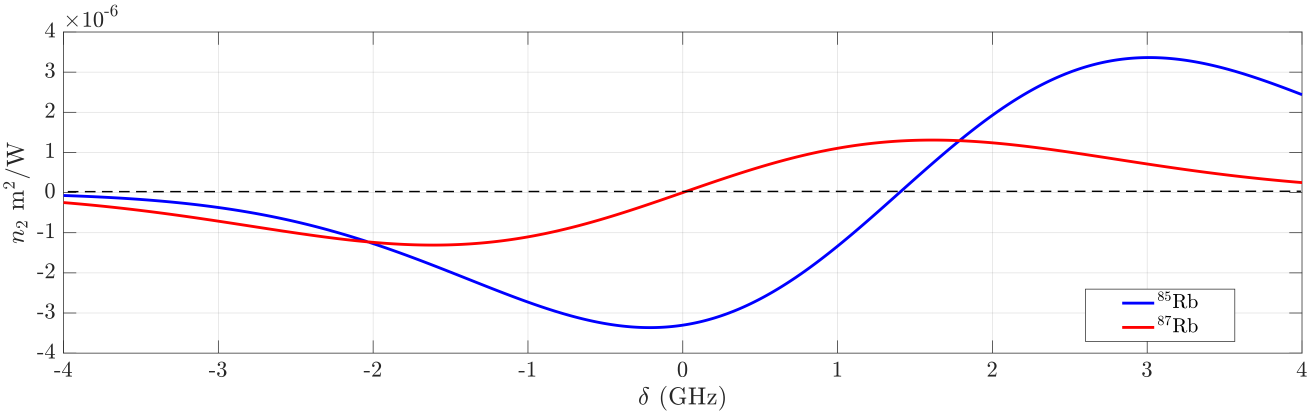

Figure 8: We plot the contribution of the two isotopes to the total value of n_2.

Now that we have obtained the variation of n_2 with δ, can we choose the parameters T, δ and I optimally? Or in other words, is the figure 7 enough for determining the optimal set of parameters for the experiment?

The answer is negative. In fact, we haven't taken into account the effect of absorption on the system. Furthermore, there is also the question of the measurement of temperature. We shall consider these two parameters in the next few sections.

6.2 Absorption

Absorption is present in any atomic system if the incident light is close to resonance. However, for atomic vapor, absorption can also occur for highly detuned incident light. Whence for n_2 the Doppler effect aided us in enlarging the range of possible δ, it limits us in the case of absorption. Since the actual detuning δ_v experienced by an atom depends on its velocity, the absorption can occur for systems far from resonance as well. Thus, the absorption coefficient itself is a function of the T, the detuning δ_v and the atomic density N.

Thus we are faced with an optimization problem: find the optimal value of Δn i.e. values of n_2, T and I while minimizing absorption in the system. However, all is not lost: we can use the absorption curve to determine the effective temperature of the system. We need to obtain an effective temperature, which is the temperature that fixes the atomic velocities. This effective temperature is not known to us by measurement of the temperature of the cell since we measure the temperature of the Rb cell at only one point. Using this effective temperature, we can compute the atomic density $N(T)$ of the system. The determination of this effective temperature proceeds by a theoretical fit to the experimental absorption spectrum.

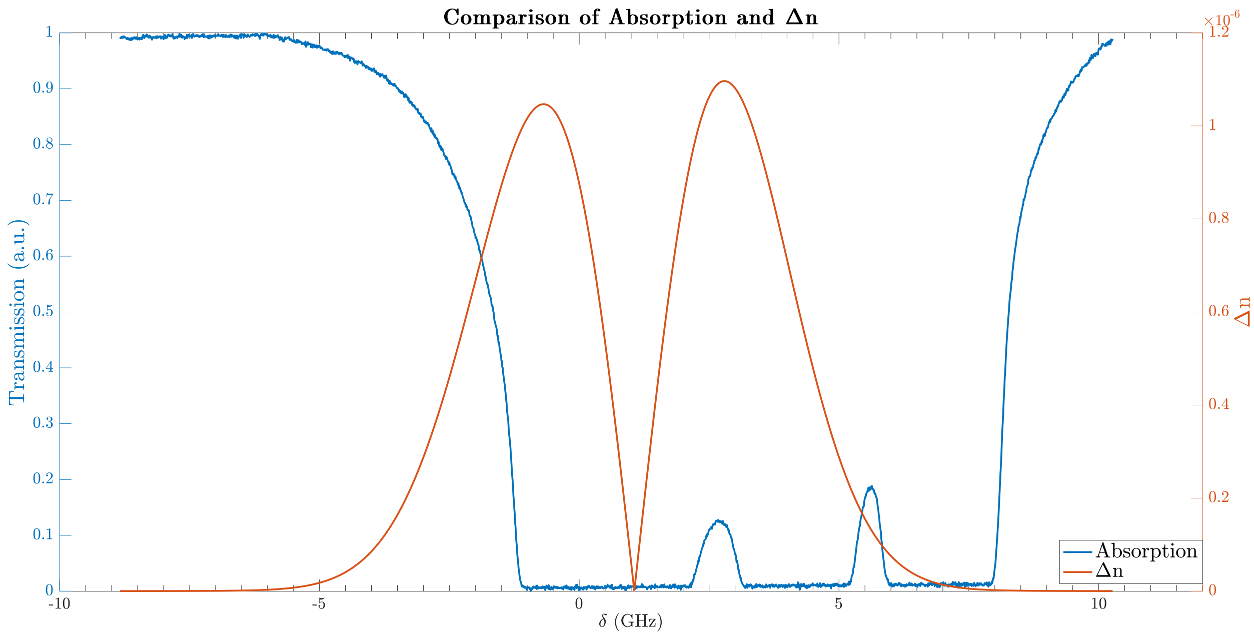

Figure 9: We note that the values of δ for which we have appreciable non-linearities are also those for which we have appreciable absorption

6.2.1 • Theoretical Model

The theoretical model for absorption in a two-level model can be written as:

$$\alpha = CN(T)\mathcal{L}(\delta) * \mathcal{N}(v), \tag{75}$$

where C is a constant, N is the atomic density, $\mathcal{L}(\delta)$ is a Lorentzian profile, typical of absorption and emission processes in two-level systems, and $\mathcal{N}(v)$ is the Gaussian distribution corresponding to the Maxwell-Boltzmann distribution for atomic velocities. Here $*$ denotes the convolution operation. We can simplify the expression for the absorption profile by using the Fourier transform, computing the relevant quantities and then performing the inverse Fourier transform [13] We get finally for the absorption profile, sans other prefactors:

$$\text{Voigt} = \frac{\sqrt{\pi}}{2}\mathrm{e}^{\frac{1}{4}(u-i2y)^2}\left(\text{Erfc}\left[\frac{u}{2} - iy\right] + \mathrm{e}^{i2uy}\text{Erfc}\left[\frac{u}{2} + iy\right]\right), \tag{76}$$

where Voigt is the voigt profile, a typical absorption profile for atomic systems. Erfc is the complimentary error function written as:

$$\text{Erfc}(z) = \frac{2}{\sqrt{\pi}}\int_z^\infty \mathrm{e}^{-t^2}\mathrm{d}t \tag{77}$$

u and y are dimensionless parameters expressed in terms of the detuning and the atomic velocity.

$$u = \frac{\Gamma}{ka}, \tag{78a}$$
$$y = \frac{\delta}{ka}, \tag{78b}$$

where a is the width of the Maxwell-Boltzmann distribution for a given temperature. The width of the Voigt profile is characterized by the parameter u, which is the ratio of the widths of the Lorentzian and Gaussian profiles. The prefactor C depends on other parameters of the atomic system, namely the line strength, the dipole moment of the two-level system considered and the degeneracy of the ground state of the respective isotope. The complete expression for the absorption coefficient is given as:

$$\alpha(\delta) = kC_F^2 d^2 N \frac{1}{2(2\mathcal{I}+1)}\frac{1}{\hbar\epsilon_0}\frac{\text{Voigt}}{ka}, \tag{79}$$

where d is the dipole moment, C_F^2 is the line strength of the particular transition and $2(2\mathcal{I}+1)$ is the degeneracy of the ground state of the isotope.

6.2.2 • Fitting procedure

The Voigt profile is the same for all hyper-fine transitions for a given isotope. The height of the Voigt profile in turn depends on the prefactors. Thus for any transition, we can compute the profile using (76), center it on the frequency corresponding to the transition and finally multiply with the corresponding prefactors to compute the theoretical absorption profile. The fit procedure then proceeds in the following fashion:

1. Select the range of detunings to take into account. For all absorption spectra, we took detunings from -9 GHz to 10 GHz. The center was always taken to be the $F = 2 \rightarrow F = 3$ transition of the ^{87}Rb D_2 line.
2. Compute the profiles for the two isotopes separately. The two isotopes have slightly different decay constants and different dipole moments.
3. For each profile, we sum the contributions from each of the hyperfine transitions. The hyperfine transitions are different in only their relative transition strengths (the term C_F^2 in (79)). Furthermore, since the incident light is linearly polarized, all three transitions are accessible.
4. The transitions are centered on the respective resonance centers.
5. The absorption spectra is then computed from Beer's law as :

$$I(z) = \mathrm{e}^{-\alpha z}, \tag{80}$$

where z is the length of the medium. In our experiment, the length of the medium corresponds to the length of the Rb cell.

6.3 Temperature T

Fitting a the theoretical Voigt profile to an experimental absorption curve is a non-linear optimisation problem. To ease this process, I designed an interactive application which runs on the browser and runs on all operating systems. This application allows us to fit many parameters such as the temperature T, and the frequency of the line centers (since there is some uncertainty about the exact values of these frequencies in the experiment). There is another panel that allows us to accurately fix the reference for the detuning.

The important parameter which is fit to the experimental curve is the temperature of the cell. As mentioned earlier, we measure the temperature of the cell at only one point of the cell and thus aren't aware of the *effective* temperature in the cell. The theoretical fit provides us this effective temperature. We also extract a calibration curve for the effective temperature as a function of the recorded temperature. We clarify however that the calibration is valid for the particular cell in use and cannot be extrapolated to other Rb cells.

The calibration curve was determined with incident intensities less than the saturation intensity of the two-level systems. The theoretical model using the voigt profile in (76) is valid only for $I < I_{\text{sat}}$. I_{sat} is defined as the optical intensity required to reduce the gain of an optical medium to half of

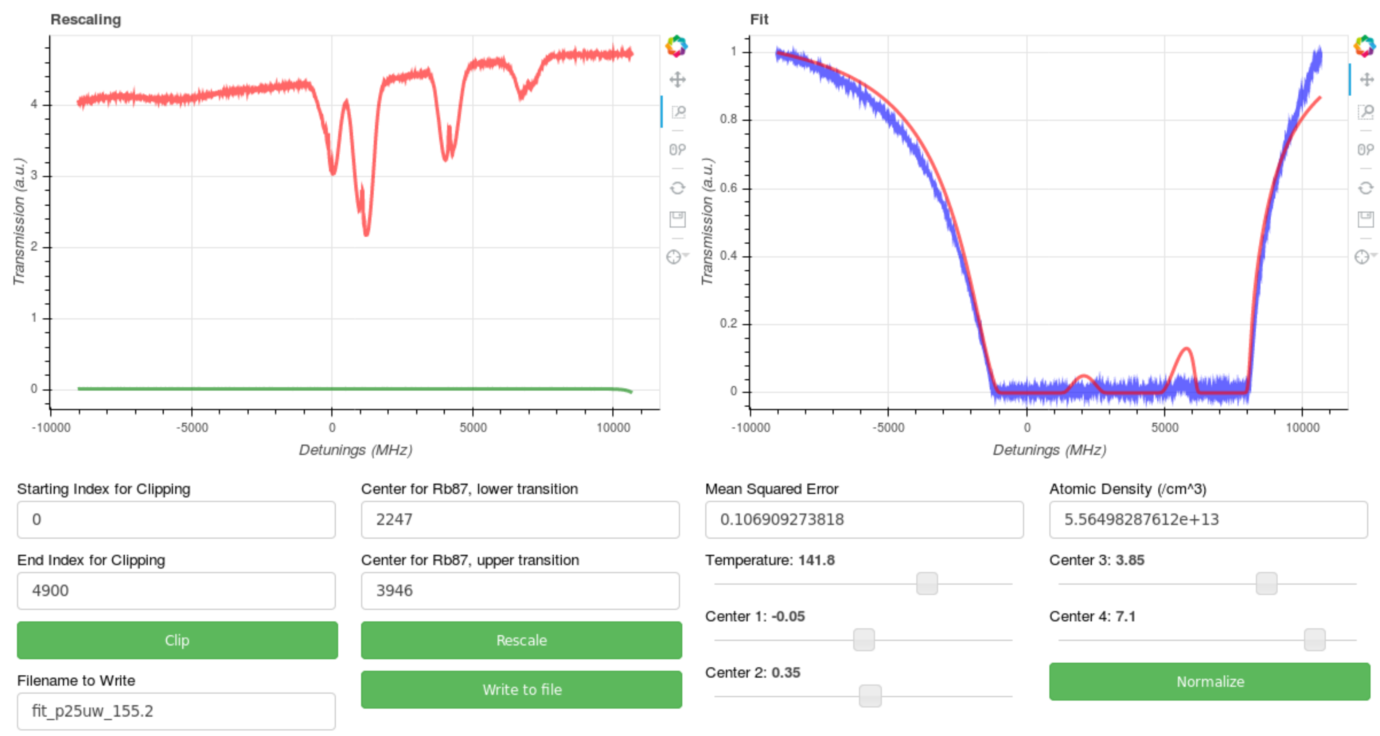

Figure 10: Interface for the fitting application

its maximum value. We can track the error between the experimental and the theoretical fit as a function of the incident intensity as shown in figure 12. We observe that for intensities less than I_{sat}, the predicted temperature is higher than that for intensities greater than I_{sat}. We conclude thus that the value of the effective temperature is valid for $I < I_{\text{sat}}$.

Computing $N(T)$

The computation of the atomic density is a straightforward using the Ideal gas law, where the pressure taken is the vapor pressure of Rb vapor in its liquid state. The calculation of $N(T)$ follows two steps:

1. Computing the vapor pressure at a given temperature (measured in Kelvin) (in our case the effective temperature) [13]

$$\log_{10} p = 15.88253 - \frac{4529.635}{T} + 0.00058663T - 2.99138 \log_{10} T. \tag{81}$$

2. Compute the atomic density

$$N = \frac{133.323p}{k_B T}. \tag{82}$$

Choosing the parameters

Once we have taken into account the absorption and its variation with δ, we can now turn our attention to choosing the values of the parameters to maximize the value of n_2. To this end, we trace out the variation of Δn (for a given intensity I) against the transmission through the Rb cell. The transmission is traced out for $\delta < 0$, since this guarantees a negative value of n_2. The choice of

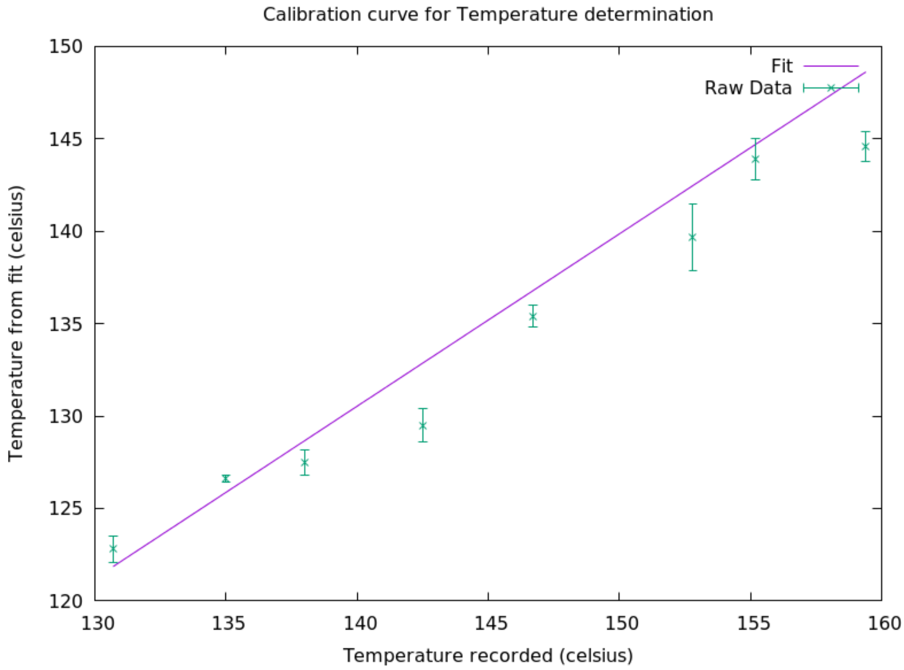

Figure 11: Calibration curve for the temperature. For each measured temperature, five absorption spectra were taken. For all absorption spectra, $I < I_{\text{sat}}$. A best-fit line of the form $f = mx$ is also plotted. This is the calibration line that is used to compute the effective *temperature from the recorded temperature.*

parameters is done by choosing the temperature which exhibits the maximum value of Δn for a fixed value of the transmission. The value of δ is then chosen for this value of Δn. Care is taken to trace out the Δn curve for the effective temperature as opposed to the recorded temperature. As presented in the figure 13, we chose a value of the transmission equal to 0.7 which fixes the value of Δn for the experiment at a given δ. We can still increase the value of Δn by increasing the intensity since Δn scales linearly with the intensity I.

7
EXPERIMENTAL SETUP

Having discussed the determination of the various parameters, we now turn our attention to the experimental setup. The experimental setup is presented below.

We can classify the different parts of the setup into three different sections:

1. Interferometer to prepare the pump and probe beams
2. Propagation through the Rb cell
3. Imaging

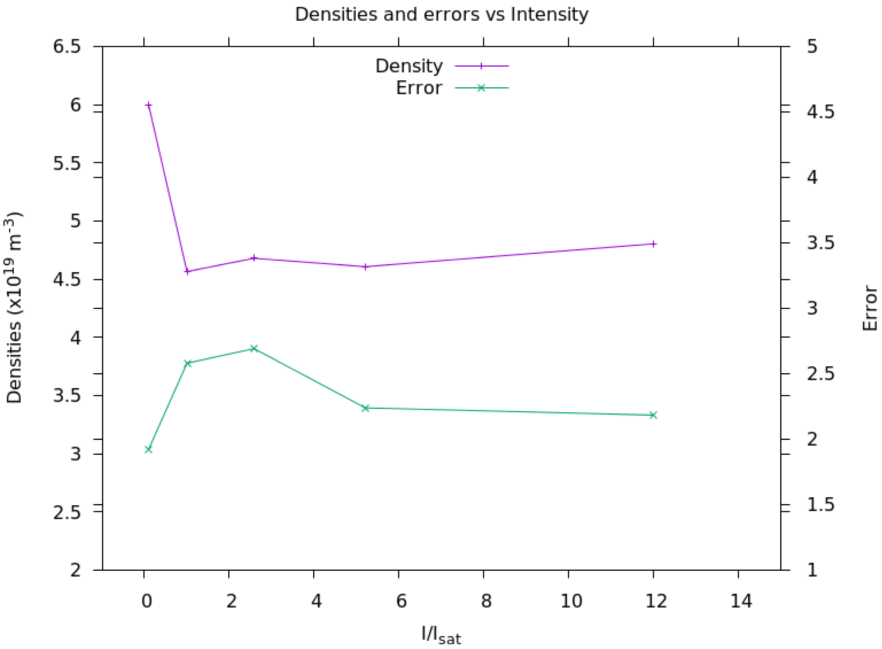

Figure 12: The densities predicted from the fit as a function of the incident intensity. We can observe the influence of the incident intensity on the error committed while fitting the experimental curve, with the least error being committed for $I < I_{\mathrm{sat}}$.

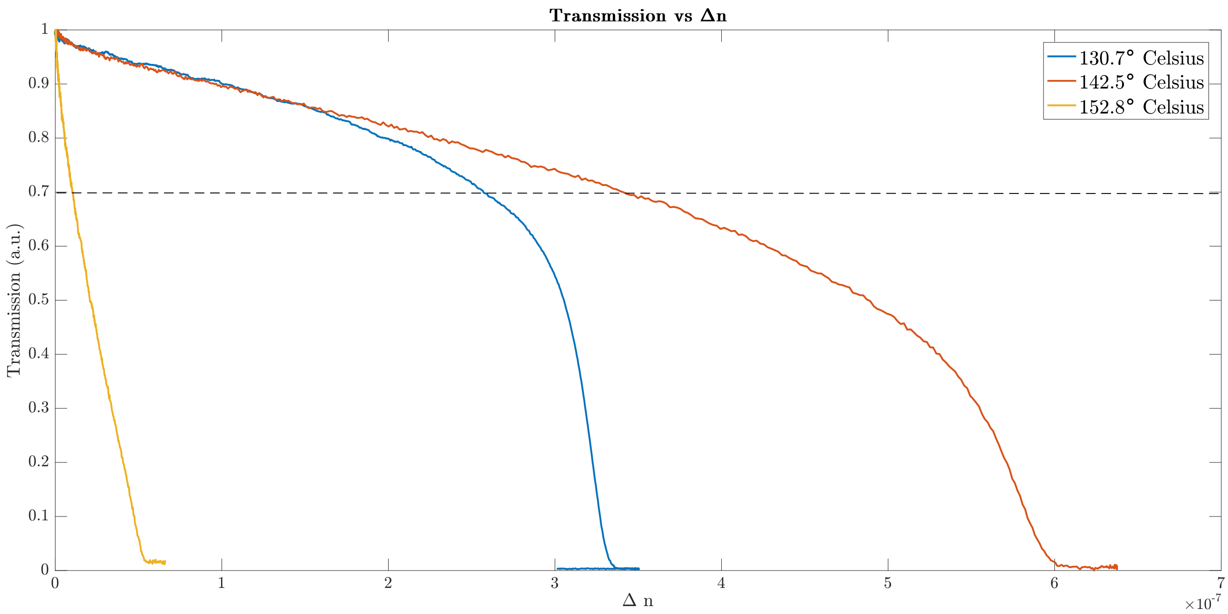

Figure 13: To choose an optimal set of parameters, we choose first the value of the temperature measured which gives us the maximum Δn for a chosen value of the transmission. Here the transmission has been fixed to 0.7. The temperatures are recorded temperatures. The values of Δn is for the effective temperature.

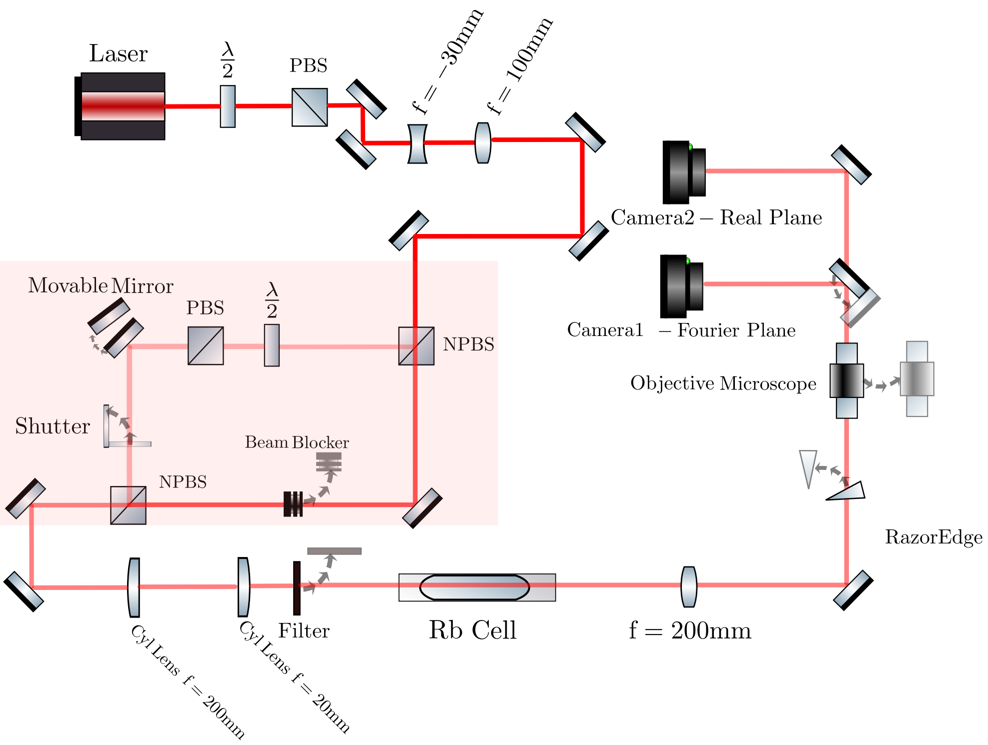

Figure 14: The complete optical setup. The part highlighted in red shows the interferometer

The section before the interferometer serves to prepare the beam before it reaches the interferometer. Using polarising beam-splitters and half wave-plates we can modulate the intensity of the beam which enters the interferometer. We shall consider each of these sections one by one.

Interferometer

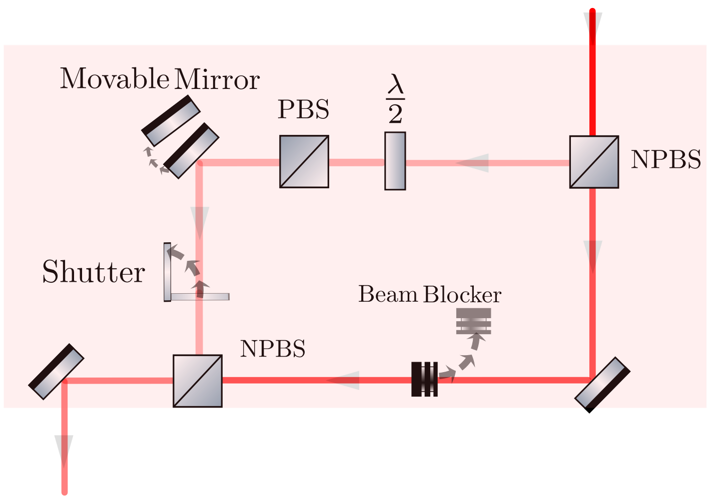

Figure 15: The interferometer

The interferometer serves to create the pump and probe beams. We create the pump and probe beams by separating a single beam using a non-polarizing beam splitter(NPBS). These beam splitters split the two beams into two coherent beams: one which carries 70% of the incident power and the other carrying 30% of the incident power. The other NPBS also splits the beam in the same manner. At the exit from the second beam-splitter, the low-intensity arm carries 9% of the initial energy, while the high-intensity arm carries 49% of the incident energy. The high-intensity arm serves as the pump beam while the other arm serves as the probe beam. On the probe arm, we also place a polarizing beam-splitter and a half wave-plate to modulate the intensity of the probe beam further. Since we require changing the angle at which the probe enters the Rb cell, we place a movable mirror, which can be controlled in three directions: one for translation along the optical table, one for changing the height of the beam (measured from the surface of the optical table) and the last one to modulate the angle of the probe beam. We place a shutter on the probe arm, allowing us to block the probe beam. A beam-blocker is placed on the pump arm as well to enable us to block the pump beam for purposes of aligning the probe beam, if required. The two beams are then recombined further at the second NPBS, which further reduces the intensity of the probe beam. We recall that we want to measure the dispersion relation of the low-amplitude excitations of the superfluid. Thus, the intensity of the probe beam is atmost 10% of that of the pump beam.

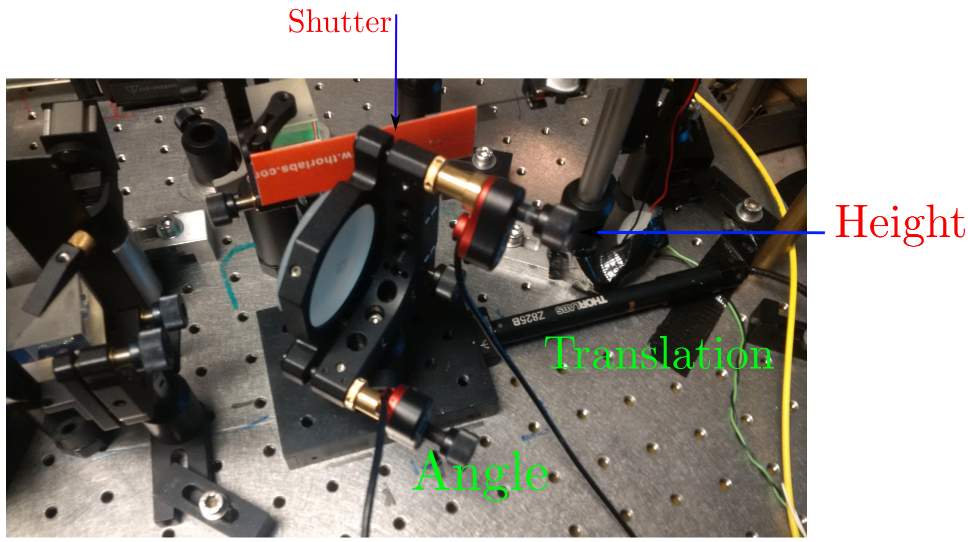

Figure 16: The movable mirror has three degrees of freedom: translation, angle and height. These three degress of freedom allow us to change the angle α between the pump and probe beams

Propagation through the cell

The pump and probe beams having interfered at the second NPBS pass through a system of two cylindrical lenses. These lenses serve to focus the beam along the $y-$axis while having a Gaussian distribution along the $x-$axis. Once transformed into an elliptical shape the two beams are then incident on the Rb cell. The Rb cell is 15 cm long and is heated uniformly along its length. We place a filter just before the cell to reduce the intensity of the incident beams. This serves to create the low-power regime for the background fluid.

Imaging

After propagation, the two beams are imaged on camera 2 which serves to image the plane at the exit face of the cell. There is another Camera used to image the Fourier Plane. We shall return to this part of the setup in a subsequent section.

8 EXPERIMENTAL PROTOCOL

The experiment proceeds through the following steps:

1. We fix a particular angle α which fixes the transverse momentum for the probe beam.
2. For this angle, we image the exit face of the Rb cell in the following configurations:
   (a) The pump beam alone in high power regime. This is achieved by removing the filter before the cell. We label this image **High-Power Background**

   (b) The pump beam alone in the low power regime. This is achieved by inserting the filter before the cell. We label this image **Low-Power Background**

   (c) The pump and probe beams with the filter removed. We label this image **High-Power Fringes**

   (d) The pump and probe beams with the filter added. We label this image **Low-Power Fringes**
3. The actual signal is extracted by subtracting the background from the images obtained in steps (c) and (d) above i.e

$$\text{High-Power Signal} = \text{High-Power Fringes - High-Power Background}$$
$$\text{Low-Power Signal} = \text{Low-Power Fringes - Low-Power Background}$$

4. The low-power signal serves as the reference with respect to which we can measure the shift induced due to the non-linear propagation in the material. The terms low-power and high-power are used to distinguish the configurations of the pump beam: with the filter present, the pump beam intensity is attenuated (thus low-power), whilst with the filter absent, the pump beam intensity is undisturbed (thus high-power).

In figure 17, we can see the difference between the low power and high power regimes. In the high power regime, we see the influence of the non-linear medium: the beam becomes defocussed. This self-defocusing can also be observed in the interference fringes that are shown in 18.

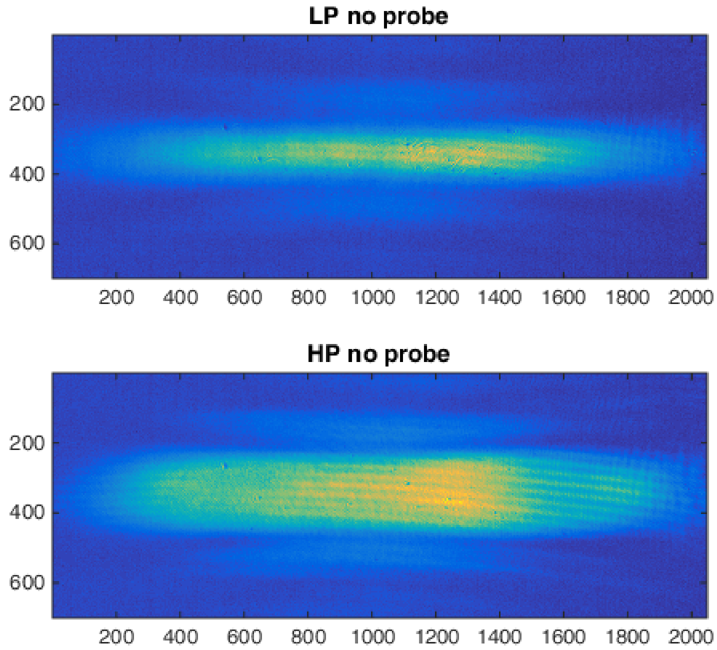

Figure 17: The pump beam imaged in the low power and high power regimes. LP denotes Low power, HP denotes High Power. In the lower panel, we can see the influence of the non-linearity: the beam becomes defocussed. This is a manifestation of $n_2 < 0$ leading to effective repulsive interactions between photons. [11]

9

DEGENERATE FOUR-WAVE MIXING

We can now extract the signal of the shift by integrating over some section of the 18. After smoothing over the signal, we get the image shown in the right panel of figure 18 What is remarkable is the absence of the shift. We observe that for the two regimes, the interference fringes are superimposed perfectly upon each other. To understand what is happening, we need to take into account a non-linear effect that we have neglected: Four-Wave Mixing.

Four wave mixing is a phenomenon which occurs in materials exhibiting $\chi^{(3)}$ non-linearity. It occurs if there are three beams of light at different (or the same) frequencies propgating within the medium. Due to the interaction between the non-linear material and the three beams of light, a fourth beam is generated whose frequency is a linear combination of the other three frequencies. In other words, if

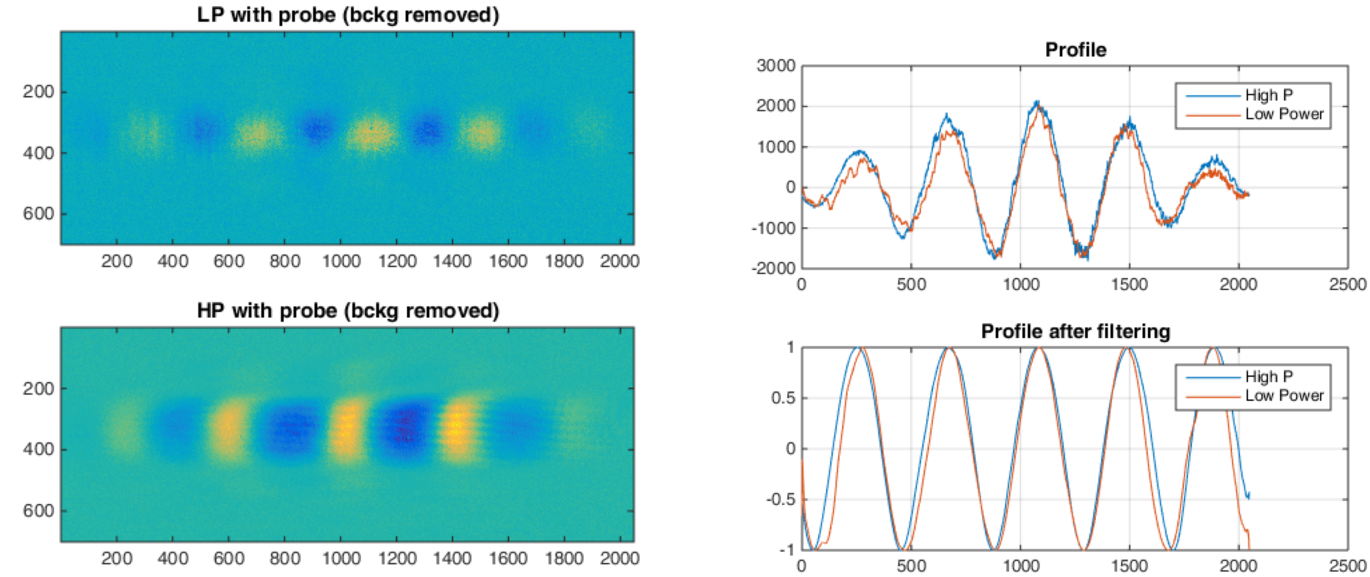

Figure 18: ***Left***: *Interference fringes with the background removed. The x and y axes are measured in pixels.* ***Right***: *ntegrated signal of the interference fringes. We choose a small region usually between 300-400 pixels from the signal in figure 18 and integrate to get the profile along the $x-$ axis. The upper panel is the integrated signal, the lower panel is the normalized and smoothed version of the integrated profile.*

ν_1 ν_2, and ν_3 are three different frequencies, the fourth beam can have a frequency

$$\nu_4 = \nu_1 + \nu_2 - \nu_3. \tag{83}$$

However, an important criteria needs to be met for the presence of this phenomena in the material: phase-matching. In other words, it doesnt suffice that the process be favorable with respect to energy conservation, it needs to be favorable with respect to *momentum* conservation as well. In other words, the process is most efficient when

$$\Delta = \vec{k}_1 + \vec{k}_2 - \vec{k}_3, \tag{84}$$

is minimal. In our experiment, we are concerned with **degenerate** four-wave mixing i.e. two photons from the pump beam interact with one photon from the probe beam to create a photon which we call the conjugate photon. The beam thus generated is called the conjugate beam. As we can see from figure 19, the efficiency of the four-wave mixing process depends on the angle between the pump and probe beams. To experimentally verify the presence of this conjugate beam, we image the Fourier transform of the exit face of the cell.

Imaging-2

The Fourier transform of the exit face can be *computed* by placing a lens at a distance of one focal length away. Then the Fourier transformed image will be formed at one focal length beyond the lens. In our setup, this is the lens which is placed right after the cell. We then place an objective microscope to magnify this Fourier transformed image, which is then imaged on camera 2. In figure 21, we can

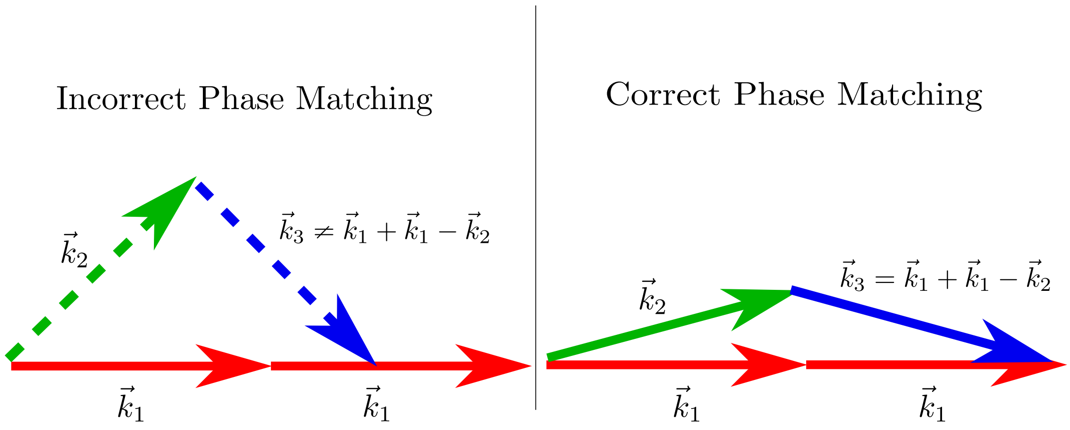

Figure 19: Phase Matching Condition for degenerate four-wave mixing. $\vec{k}_1$ is the wave-vector for the pump beam, $\vec{k}_2$ for the probe beam and $\vec{k}_3$ for the conjugate beam. We remark the importance of the angle between the pump and probe beams: if the angle is too large, the conjugate beam is not perfectly phase-matched and thus the four-wave mixing process isn't efficient. However, for smaller angles, phase-matching is easier and the conjugate beam has an appreciable intensity.

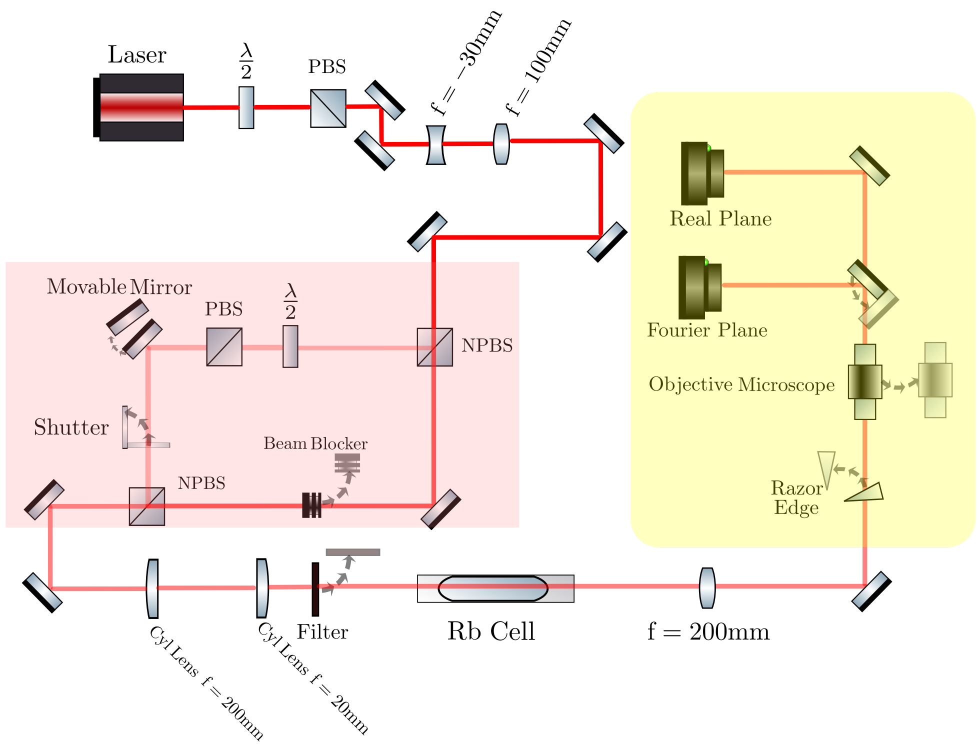

Figure 20: We recall the optical setup with the section on imaging highlighted in yellow.

observe the generation of the conjugate beam. We also observe that the conjugate beam is generated symmetrically with respect to the probe beam. The generation of the conjugate beam explains the absence of the shift which was observed in figure 18.

The reason is rather simple: for small angles, the process of the generation of the conjugate beam is very efficient. If we consider the interference of the pump beam with the conjugate beam, then we expect the presence of a shift between the reference pattern and the high-power pattern. However, the conjugate beam is generated symmetrically to the probe beam. This implies that if the probe beam is at an angle α to the pump, the conjugate beam is generated at an angle $-\alpha$ to the pump. Thus if the shift due to the presence of the probe beam is towards the right, the shift due to the conjugate beam will be towards the left. The result will be a net zero shift as observed in figure 18.

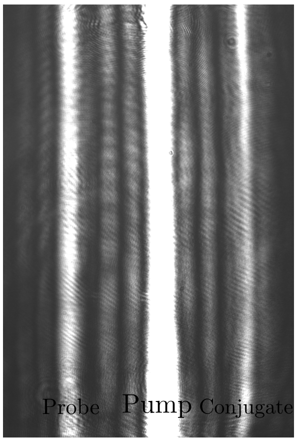

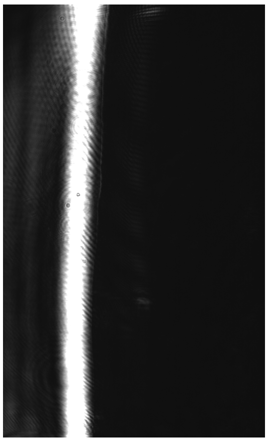

Figure 21: ***Left****:On the Fourier plane, we have separated the pump, probe and conjugate beams. We remark the symmetric generation of the conjugate beam. Furthermore, the intensity of the conjugate beam is comparable to that of the probe beam.* ***Right****:The razor edge completely covers the right part of the Fourier Plane masking the conjugate beam.*

To observe the shift, we need to filter out the conjugate beam. To this end, we use a razor edge, as shown in the optical setup (figure 20). The razor edge is placed such that the conjugate beam is completely blocked. We place the razor edge in the Fourier plane. The imaging for the interference fringes is done in the real plane on camera 1. To enable us to switch from the real to the Fourier plane, we place a flip-mirror after the objective microscope. An image of the Fourier plane with the razor edge is shown in figure 21.

Once the conjugate beam has been masked out, we return to imaging the exit face (the real plane). We observe the shift in the interference pattern that was predicted from theory in figure 22.

10

EXPERIMENTAL RESULTS

After having corrected for degenerate four-wave mixing, we conducted the experiments for the following parameters:

1. $\delta = 2.0$ GHz
2. $T_{\text{measured}} = 142.5°$ Celsius
3. $P_{\text{incident}} = 200$mW

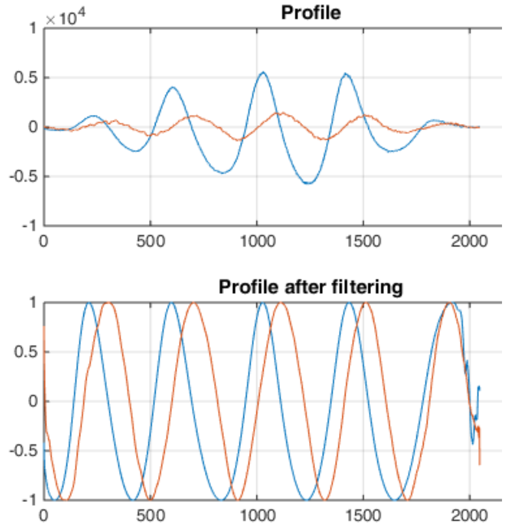

Figure 22: Integrated signal after masking the conjugate beam. We now observe the shift between the interference patterns as predicted from theory. The x-axis represents the number of pixels on the camera. The y-axis in the top panel has arbitrary units.

For these parameters, $\Delta n \approx 1.2 \times 10^{-6}$. After performing the experiment for these parameters, we get the following results:

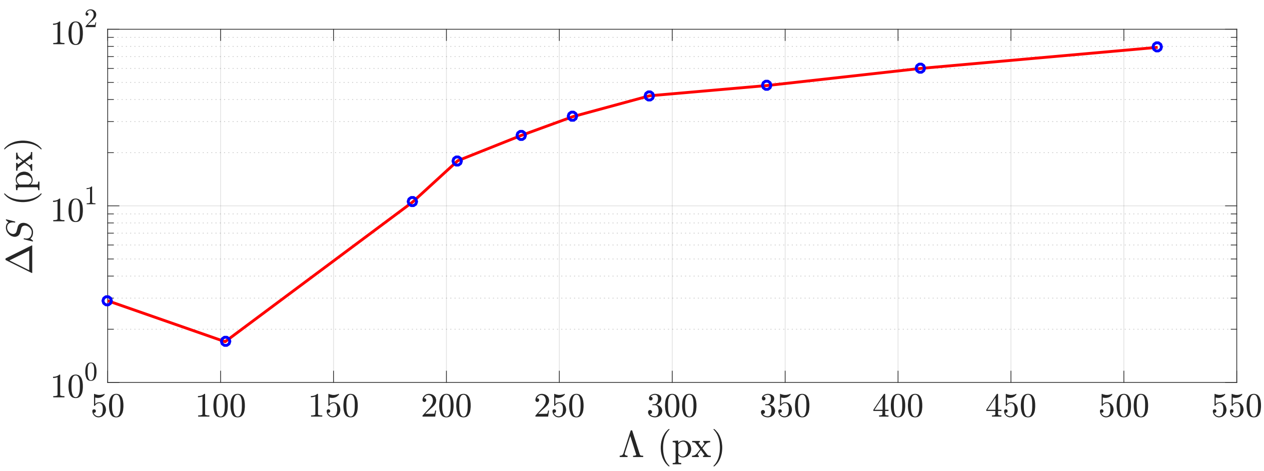

Figure 23: The experimental curve of the shift ΔS vs Λ performed with the parameters indicated above. We observe the saturation of the shift for higher values of Λ.

Figure 23 shows the preliminary results for the measurement of the shift ΔS. This preliminary curve is the first demonstration of superfluigity in light using an atomic vapor. The shift and Λ are calculated on the central fringe.

Note on the results

The data was taken for 17 different values of Λ whereas in figure 23, we have presented the results only for 10 values. A complete and thorough analysis has not been performed for the rest of the data.

We are hopeful that with more data points with higher values of Λ, we will be able to demonstrate unequivocally superfluidity in light.

Part IV

Conclusion and Future Perspectives

We have demonstrated how the propagation of light in a non-linear medium can be used to simulate superfluidity. The enormous interest of this approach is the simplicity of the experimental protocol. However, we do need to take into account other non-linear effects such as absorption, Doppler broadening, self-defocusing and degenerate four-wave mixing. One of the principal contributions of the work presented here is a comprehensive understanding of all these non-linear phenomena, which will allow further investigation to be carried out rapidly. Finally, The first experimental results obtained and presented here are promising.

Some future perspectives:

1. **Extending the pump-probe technique to study the flow of two *superfluids***: The pump-probe technique presented here works with a weak probe beam. By increasing the intensity of the probe beam (or by tuning some other parameter), we can use the probe beam as a superfluid as well (by increasing the non-linearity). In such a case, we can study the flow of two superfluids, one formed by the pump and the other by the probe. This provides a novel way for studying the mixture of superfluids by using simpler optical systems.

2. **Including potential terms**: The analogy of the non-linear propagation of light and the Gross-Pitaevskii equation studied here assumed the absence of potential terms. For optical systems such as ours, we can induce a discontinuity in the local refractive index, which can serve as an obstacle for the propagation of light. This is a particularly exciting experiment to perform since this provides a direct confirmation of superfluid flow: the passage from normal fluid flow to superfluid flow is characterized by the absence of the creation of turbulent vortices around obstacles.

3. **Increasing the non-linearity**

   (a) Reducing the length of the cell: BY reducing the length of the cell, we can decrease the absorption. This allows to access detunings closer to zero, leading to enhanced non-linearities.

   (b) Electromagnetically Induced Transparency: This is a non-linear effect, which renders a medium transparent within a narrow band of frequencies within an absorption line. We can thus envisage to utilise EIT to make the medium transparent close to the peak of the $|\Delta n|$ curve.

REFERENCES

[1] J. F. Allen and A. D. Misener. "Flow Phenomena in Liquid Helium II". In: *Nature* 142.3597 (1938), pp. 643–644. DOI: 10.1038/142643a0.

[2] P. Kapitza. "Viscosity of Liquid Helium below the λ-Point". In: *Nature* 141.3558 (1938), pp. 74–74. DOI: 10.1038/141074a0.

[3] F. London. "The λ-Phenomenon of Liquid Helium and the Bose-Einstein Degeneracy". In: *Nature* 141.3571 (1938), pp. 643–644. DOI: 10.1038/141643a0.

[4] Martin Weitz, Jan Klaers, and Frank Vewinger. "Optomechanical generation of a photonic Bose-Einstein condensate". In: *Physical Review A* 88.4 (2013), p. 045601. DOI: 10.1103/PhysRevA.88.045601.

[5] Alberto Amo et al. "Superfluidity of polaritons in semiconductor microcavities". In: *Nature Physics* 5.11 (Nov. 2009), pp. 805–810. DOI: 10.1038/nphys1364.

[6] T. Boulier et al. "Injection of Orbital Angular Momentum and Storage of Quantized Vortices in Polariton Superfluids". In: *Physical Review Letters* 116.11 (2016), p. 116402. DOI: 10.1103/PhysRevLett.116.116402.

[7] Jean Dalibard et al. "Colloquium : Artificial gauge potentials for neutral atoms". In: *Reviews of Modern Physics* 83.4 (Nov. 2011), pp. 1523–1543. DOI: 10.1103/RevModPhys.83.1523.

[8] P E Larré et al. "Quantum fluctuations around black hole horizons in Bose-Einstein condensates". In: *Physical Review A* 85 (2012), pp. 13621–70. DOI: 10.1103/PhysRevA.85.013621.

[9] Lev Pitaevskii and Sandro Stringari. *Bose-Einstein Condensation*. Vol. 116. 3. 2003, p. 492. ISBN: 0198507194.

[10] M. Born and E. Wolf. *Principles of optics*. 1999. DOI: 10.1016/S0030-3992(00)00061-X.

[11] Robert W Boyd. "Nonlinear Optics". In: *Applied Optics* 5 (2003), p. 578. DOI: 10.1109/NLO.1990.695958. arXiv: 0102038 [physics].

[12] David Vocke et al. "Experimental characterization of nonlocal photon fluids". In: *Optica* 2.5 (2015), p. 484. DOI: 10.1364/OPTICA.2.000484.

[13] Paul Siddons et al. "Absolute absorption on the rubidium D lines: comparison between theory and experiment". In: *Journal of Physics B: Atomic, Molecular and Optical Physics* 41.15 (2008), p. 155004. DOI: 10.1088/0953-4075/41/15/155004.